AD-A010 103

DEVELOPMENT OF THERMOCOUPLE GENERATORS FOR SMALL-CALIBER MUNITIONS FUZE. PHASE I

Philip E. Eggers

Battelle Columbus Laboratories

Prepared for:

Aerospace Research Laboratories

March 1975

DISTRIBUTED BY:

NTIS

National Technical Information Service
U. S. DEPARTMENT OF COMMERCE

AD A010103

155094

AD1 12 75-0073

DEVELOPMENT OF THERMOCOUPLE GENERATORS FOR SMALL-CALIBER MUNITIONS FUZE

PHASE I

PHILIP E. EGGERS

BATTELLE
COLUMBUS LABORATORIES
505 KING AVENUE
COLUMBUS, OHIO 43201

DDC
RECEIVED
MAY 27 1975
A

MARCH 1975

FINAL REPORT 1 FEBRUARY 1974 — 3 SEPTEMBER 1974

Approved for public release; distribution unlimited

Reproduced by
NATIONAL TECHNICAL
INFORMATION SERVICE
US Department of Commerce
Springfield, VA. 22151

ENERGY CONVERSION RESEARCH LABORATORIES/LE
AEROSPACE RESEARCH LABORATORIES
Building 400 — Area B
Wright-Patterson Air Force Base, Ohio 45433

AIR FORCE SYSTEMS COMMAND
United States Air Force

NOTICES

When Government drawings, specifications, or other data are used for any purpose other than in connection with a definitely related Government procurement operation, the United States Government thereby incurs no responsibility nor any obligation whatsoever; and the fact that the Government may have formulated, furnished, or in any way supplied the said drawings, specifications, or other data, is not to be regarded by implication or otherwise as in any manner licensing the holder or any other person or corporation, or conveying any rights or permission to manufacture, use, or sell any patented invention that may in any way be related thereto.

Organizations or individuals receiving reports via Aerospace Research Laboratories automatic mailing lists should refer to the ARL number of the report received when corresponding about change of address or cancellation. Such changes should be directed to the specific laboratory orginating the report. Do not return this copy; retain or destroy.

Reports are not stocked by the Aerospace Research Laboratories. Copies may be obtained from:

National Technical Information Services
Clearinghouse
Springfield, VA 22151

This technical report has been reviewed and is approved for publication.

FOR THE COMMANDER:

Elizabeth Day

ELIZABETH DAY
Technical Documents
and STINFO Office

ACCESSION for
NTIS White Section
DDC Buff Section
UNANNOUNCED
JUSTIFICATION
BY
DISTRIBUTION/AVAILABILITY CODES
Dist. AVAIL. and/or SPECIAL
A

This report has been reviewed and cleared for open publication and public release by the appropriate Office of Information in accordance with AFR 190-12 and DODD 5230.0. There is no objection to unlimited distribution of this report to the public at large, or by DDC to the National Technical Information Service.

AIR FORCE/56780/30 April 1975 — 200

UNCLASSIFIED

SECURITY CLASSIFICATION OF THIS PAGE (When Data Entered)

REPORT DOCUMENTATION PAGE

READ INSTRUCTIONS BEFORE COMPLETING FORM

1. REPORT NUMBER: ARL 75-0013

2. GOVT ACCESSION NO.:

3. RECIPIENT'S CATALOG NUMBER: AD-A010 103

4. TITLE (and Subtitle): DEVELOPMENT OF THERMOCOUPLE GENERATORS FOR SMALL-CALIBER MUNITIONS FUZE

5. TYPE OF REPORT & PERIOD COVERED: Technical - Final, 1 Feb 74- 3 Sep 74

6. PERFORMING ORG. REPORT NUMBER:

7. AUTHOR(s): Philip E. Eggers

8. CONTRACT OR GRANT NUMBER(s): F33615-74-C-4043

9. PERFORMING ORGANIZATION NAME AND ADDRESS:
Battelle
Columbus Laboratories
505 King Avenue, Columbus, Ohio 43201

10. PROGRAM ELEMENT, PROJECT, TASK AREA & WORK UNIT NUMBERS:
61102F
71160208

11. CONTROLLING OFFICE NAME AND ADDRESS:
Energy Conversion Research Laboratory (LE)
Aerospace Research Laboratories (AFSC)
Wright-Patterson AFB, Ohio 45433

12. REPORT DATE: March 1975

13. NUMBER OF PAGES: 80

14. MONITORING AGENCY NAME & ADDRESS (if different from Controlling Office):

15. SECURITY CLASS. (of this report): Unclassified

15a. DECLASSIFICATION/DOWNGRADING SCHEDULE:

16. DISTRIBUTION STATEMENT (of this Report):

Approved for public release; distribution unlimited.

17. DISTRIBUTION STATEMENT (of the abstract entered in Block 20, if different from Report):

18. SUPPLEMENTARY NOTES:

19. KEY WORDS (Continue on reverse side if necessary and identify by block number):

thermoelectrics	proximity fuze
thermopiles	projectile
aerodynamic heating	sputtering
thin film	transient thermal analysis

20. ABSTRACT (Continue on reverse side if necessary and identify by block number):

An analytical study has been performed to assess the feasibility of utilizing aerodynamically heated thermoelectric convertors to power RF proximity fuzes. The collective results of this study indicate that such a thermoelectric power supply is feasible for use with 20 mm projectiles and is compatible with the existing RF fuze circuit and safe arming distance requirements. A disc module concept has evolved from this study involving thin-film bismuth telluride as the basic thermoelectric element. Preliminary experimental studies were completed in order to identify principal parameters for the bismuth telluride sputtering process.

DD FORM 1 JAN 73 1473 EDITION OF 1 NOV 65 IS OBSOLETE

UNCLASSIFIED

SECURITY CLASSIFICATION OF THIS PAGE (When Data Entered)

PREFACE

This is the final report on research conducted at Battelle's Columbus Laboratories, Columbus, Ohio, on Project G2756 under United States Air Force Contract No. F33615-74-C-4043 during the period 1 February 1974 to 3 September 1974.

The Air Force project monitor for this contract was Lt. James M. Howard, Energy Conversion Research Laboratory (LE), Aerospace Research Laboratories (AFSC), Wright-Patterson Air Force Base, Ohio 45433.

The principal investigator for Battelle's Columbus Laboratories was Philip E. Eggers. Contributions to the research effort were also made by R. H. Blazek, J. L. Corliss, W. E. Gawthrop, I. Grinberg, S. Goddard, V. Levin, J. J. Mueller, F. A. Simonen, G. H. Stickford, and C. T. Wan.

TABLE OF CONTENTS

SECTION		PAGE
I	INTRODUCTION	1
	1. REVIEW OF PREVIOUS FUZE DEVELOPMENT EFFORTS	1
	2. OUTLINE OF RESEARCH APPROACH	2
II	POWER REQUIREMENTS OF PROXIMITY FUZE CIRCUIT INVOLVING THERMOELECTRIC POWER SOURCE	5
	1. CHARACTERIZATION OF ORIGINAL FUZE CIRCUIT DESIGN	5
	2. DESCRIPTION OF MODIFIED PROXIMITY FUZE CIRCUIT	7
	3. FUZE CIRCUIT POWER REQUIREMENTS	9
III	IDENTIFICATION OF CANDIDATE THERMOPILE CONFIGURATION AND ASSOCIATED MATERIALS	13
	1. SELECTION OF RANGE FOR PARAMETERS	
	a. Thermoelectric Materials	13
	b. Temperature Difference	15
	c. Thermoelement Length	15
	d. Thickness of Thermoelements	15
	2. SELECTION OF THERMOPILE CONFIGURATION	15
	3. SELECTION OF CANDIDATE THERMOPILE DESIGN	16
IV	AERODYNAMIC HEATING ANALYSIS	19
	1. BLUNT CONE CONFIGURATION	19
	2. LAMINAR BOUNDARY LAYER HEAT TRANSFER	19
	3. PROJECTILE SPIN EFFECTS	21
	4. BOUNDARY LAYER TRANSITION	23
	5. RESULTS OF BOUNDARY LAYER HEATING CALCULATIONS	24
V	OPTIMIZATION OF THERMOPILE DESIGN	31
	1. DESCRIPTION OF THERMAL MODEL	33
	2. THERMAL ANALYSIS OF DISC CONVERTER FOR SELECTED SUBSTRATE MATERIALS	34

Preceding page blank

TABLE OF CONTENTS (CONTINUED)

SECTION		PAGE
	3. TEMPERATURE DIFFERENCE ACROSS CONVERTER AS A FUNCTION OF TIME	36
	4. OUTPUT POWER AS A FUNCTION OF TIME	36
	5. SENSITIVITY OF THERMOPILE TEMPERATURE DIFFERENCE AND OUTPUT POWER TO MUZZLE VELOCITY	40
	6. SENSITIVITY OF THERMOPILE TEMPERATURE DIFFERENCE AND OUTPUT POWER TO ALTITUDE AT FIRING	41
	7. CIRCUIT ANALYSIS OF FUZE CIRCUIT POWERED BY THERMOELECTRIC CONVERTER	43
	8. ADVANTAGES AND LIMITATIONS OF ENERGY STORAGE IN RF PROXIMITY FUZES	46
VI	STRUCTURAL ANALYSIS OF DISC THERMOELECTRIC CONVERTOR	49
	1. ANALYTICAL APPROACH	49
	2. ROTATIONAL STRESSES	50
	3. ACCELERATION STRESSES	50
	4. THERMAL STRESSES	51
	5. COMMENTS ON STRUCTURAL INTEGRITY	51
VII	DYNAMIC STABILITY ANALYSIS	52
VIII	COST EFFECTIVENESS OF THERMOELECTRIC CONVERTER	57
IX	SAFETY ANALYSIS	63
X	CONCLUSIONS AND RECOMMENDATIONS	65
	REFERENCES	68
	APPENDIX A: DESCRIPTION OF THE COMPUTER PROGRAM TRUMP	69

LIST OF TABLES

TABLE		PAGE
I	SUMMARY OF THERMOELECTRIC CONVERTER CHARACTERISTICS FOR SELECTED SEMICONDUCTOR AND SEMIMETAL MATERIALS	14
II	COMPARISON OF PEAK TEMPERATURE DIFFERENCES ACROSS THERMOELEMENTS FOR SELECTED SUBSTRATE MATERIALS.	35
III	VARIATION IN TEMPERATURE DIFFERENCE AND OUTPUT POWER AS A FUNCTION OF MUZZLE VELOCITY FOR 20MM PROJECTILE . . .	42
IV	RELATIONSHIP OF FIRING CONDITIONS WITH PROXIMITY FUZE CIRCUIT PERFORMANCE	45
V	PARTIAL DERIVATIVES FOR DETERMINING λp (SEA LEVEL)	54
VI	PARTIAL DERIVATIVES FOR DETERMINING S_g^{-1} (SEA LEVEL) . . .	54
VII	PARTIAL DERIVATIVES FOR DETERMINING S_d (SEA LEVEL)	54
VIII	EFFECT OF MASS PROPERTY CHANGES ON THE STABILITY PARAMETERS.	54
IX	APPROXIMATE COST BREAKDOWN FOR DISC THERMOELECTRIC CONVERTORS	62

LIST OF ILLUSTRATIONS

FIGURE		PAGE
1	Schematic Diagram of Research Program for the Development of Aerodynamically Heated Thermoelectric-Power Supplies for RF Proximity Fuzes . . .	4
2	Schematic Diagram of RF Proximity Fuze	6
3	Detonator Firing Requirements.	8
4	Revised Fuze Circuit (Supply Voltage, 7V).	10
5	Fuse Circuit (Supply Voltage, 11 V).	11
6	Disc-Shaped Thermoelectric Module Concept Featuring Thin-Film Thermoelements	17
7	Cross-Sectional View of 20 mm Projectile Involving Disc Thermoelectric Modules.	18
8	Schematic of Blunt Cone Flow Field Typical of 20mm Projectile	20
9	Comparison of Experimental Data With Theory for Laminar Flow Over a Blunted Cone, Ref 1.	22
10	Comparison of Transition Correlation with Data for Ballistics Range.	25
11	Altitude-Mach No. Map for 20mm Projectile Fired From Various Vehicles	26
12	Results of Trajectory Calculation from RETAS Code.	27
13	Distributed Heating on 20mm Projectile	28
14	Aerodynamic Heating of 20 mm Projectile at a Point 1.5 cm From Tip For a Firing Angle of -20 Degrees	30
15	Thermal Model of Disc Thermoelectric Converter Concept . .	32
16	Temperature Difference Across Convertor as a Function of Time.	37

LIST OF ILLUSTRATIONS (CONTINUED)

FIGURE		PAGE
17	Convertor Open Circuit Voltage as a Function of Elapsed Time	38
18	Convertor Output Power as a Function of Time	39
19	Temperature Difference Across the Thermoelectric Convertor for Selected Hot Strap Thicknesses	48
20	Stability Plot, S_g^{-1} vs S_d	56
21	Photograph of Sputtered Bismuth Telluride Films (0.100 in. Long x 0.025 in. Wide x 0.0005 in. Thick).	60

SECTION I

INTRODUCTION

The development of miniaturized solid state sensors and associated electronics has permitted design of radar proximity fuzes for use in small caliber, high explosive projectiles. However, the development of miniaturized power supplies has not been commensurate with advances in micro-electronic technology. Miniaturized thermoelectric generators for converting projectile aerodynamic heating into electricity to power electronic microcircuits may provide advantages, especially shelf-life and safety, in armament fuzing applications. While the results of this effort are intended to be applied directly to a 20 mm projectile fired from an aircraft, indications are that there are many other applications in munitions.

1. REVIEW OF PREVIOUS FUZE DEVELOPMENT EFFORTS

The Air Force demonstrated the feasibility of producing a radar proximity fuze for a small caliber (20 mm) projectile under Contract F08635-71-C-0154. As a result of this effort, the micro-electronics for a small cw doppler radar proximity fuze were developed, and 38 prototype fuzes were produced and test fired. In order to demonstrate the operation of the electronics circuit, stored energy in the form of a small spin-activated battery was used as a power source.

The Air Force also sponsored work under Contract F08635-72-C-0012 to study, refine, and characterize a power converter nose cone using thermoelectric energy conversion techniques to transform aerodynamic heating into the required electrical power.[1] This contract was directed primarily towards the identification of potential applications for thermoelectric generators, the study of thermoelectric material characteristics, and possible manufacturing technology

for thermoelectric generators. It was apparent from this preliminary study that further research was needed to define projectile surface heating rates, establish an optimum thermopile design, and to evaluate mechanical suitability and projected costs of such a power source.

2. OUTLINE OF RESEARCH APPROACH

The overall objective of this Phase I study was to evaluate the feasibility of aerodynamically heated thermoelectric-power supplies suitable for use in small caliber fuzes. To this end, Battelle conducted a program consisting of eight tasks as summarized below:

- In the first period of Phase I, the principal technology groups associated with this project were integrated into a team to review the possible candidate thermopile designs and to establish realistic "bounds" for the subsequent analytical phase. (This is represented schematically as Tasks I and II in Figure 1.)
- In the second period of Phase I the thermopile analytical effort was partioned into distinct (yet interacting) areas of consideration such as aerodynamic heating, thermoelectric design optimization, mechanical suitability, cost effectiveness, and safety (see Tasks III through VII in Figure 1).
- In the second phase of this study (if continued) BCL plans to focus its effort on prototype hardware development based on the collective results of the first phase.

Although the analysis in the Phase I study was partitioned according to the principal area of consideration, each analysis remained interactive with respect to the other system design considerations. In this way, the development of the "optimum" thermopile progressed through a hierarchy of design considerations in which the thermopile design becomes further refined at each successive level. As indicated in Figure 1 (see Task III), the initial level of the hierarchy involved that phase of the design optimization which is

dictated by the given mission and, hence, least flexible. The next level of the hierarchy (see Figure 1, Task IV) involved the thermoelectric design optimization analysis which is also relatively inflexible due to the limited number of available materials which meet the thermoelectric energy conversion requirements.

The discussion which follows has been divided into sections according to the tasks outlined in Figure 1.

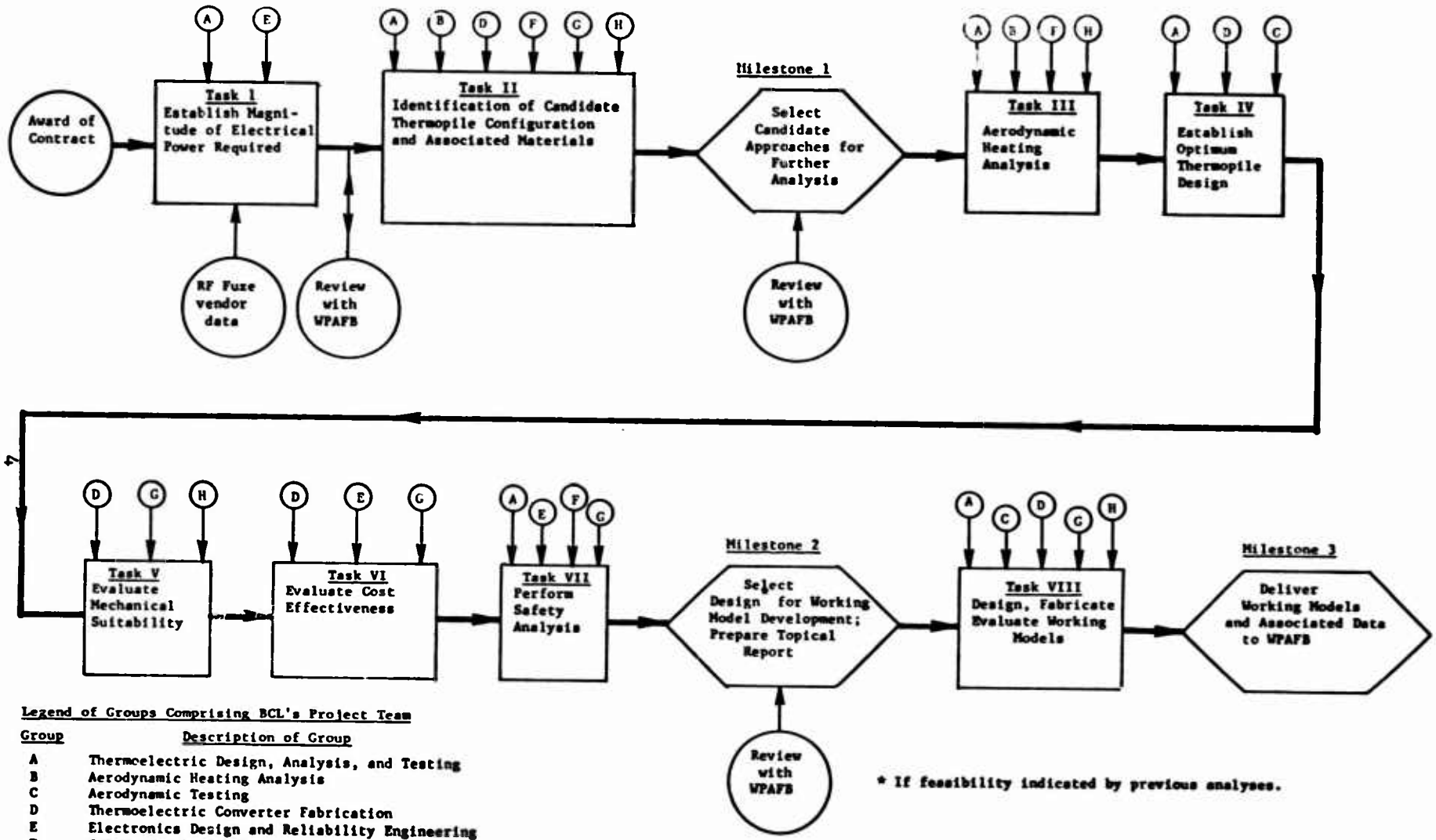

Legend of Groups Comprising BCL's Project Team

Group	Description of Group
A	Thermoelectric Design, Analysis, and Testing
B	Aerodynamic Heating Analysis
C	Aerodynamic Testing
D	Thermoelectric Converter Fabrication
E	Electronics Design and Reliability Engineering
F	Conventional Weapons
G	Ordnance Fabrication Technology
H	Structural and Thermal Stress Analysis.

FIGURE 1. SCHEMATIC DIAGRAM OF RESEARCH PROGRAM FOR THE DEVELOPMENT OF AERODYNAMICALLY HEATED THERMOELECTRIC-POWER SUPPLIES FOR RF PROXIMITY FUZES

SECTION II

POWER REQUIREMENTS OF PROXIMITY FUZE CIRCUIT INVOLVING THERMOELECTRIC POWER SOURCE

The objective of this task was to determine the power requirements of the proximity fuze circuit involving an aerodynamically heated thermoelectric power source.

A fuze circuit was developed under a previous contract involving[1] power requirements of about 300 mw. However, the proximity fuze circuit power requirements need to be reduced to 60 mw or less in order to be feasible for operation with an aerodynamically heated thermoelectric power source.

1. CHARACTERIZATION OF ORIGINAL FUZE CIRCUIT DESIGN

The characterization of the original fuze circuit was initiated after receipt of a unclassified version of the contractor report[2] entitled "Air to Surface Proximity Fuze for 20mm Projectile", which described the fuze circuit development and testing.

The fuze circuit developed in the previous work is shown in Figure 2. It consists of an oscillator and an antenna, signal detector, amplifier, impact switch, a time delay circuit, and a voltage regulator. The oscillator consists of transistor, Q_1, coil, L_1, and the collector/emitter capacitance of transistor Q_1. The oscillator output is coupled to the antenna and transmitted. The return signal is received by the quarter wave antenna across the emitter resistor, R_2. This voltage is coupled through a 47 nF capacitor to the inverting (-) input of the operational amplifier while the non-inverting (+) input is connected to the base of the transistor, Q_1. Therefore, this input always sees a positive voltage which never exceeds 2.1 volts, i.e., the sum of the voltage drops for the three diodes, DS1. This permits the operational amplifier to act as a voltage follower and to operate from a single battery

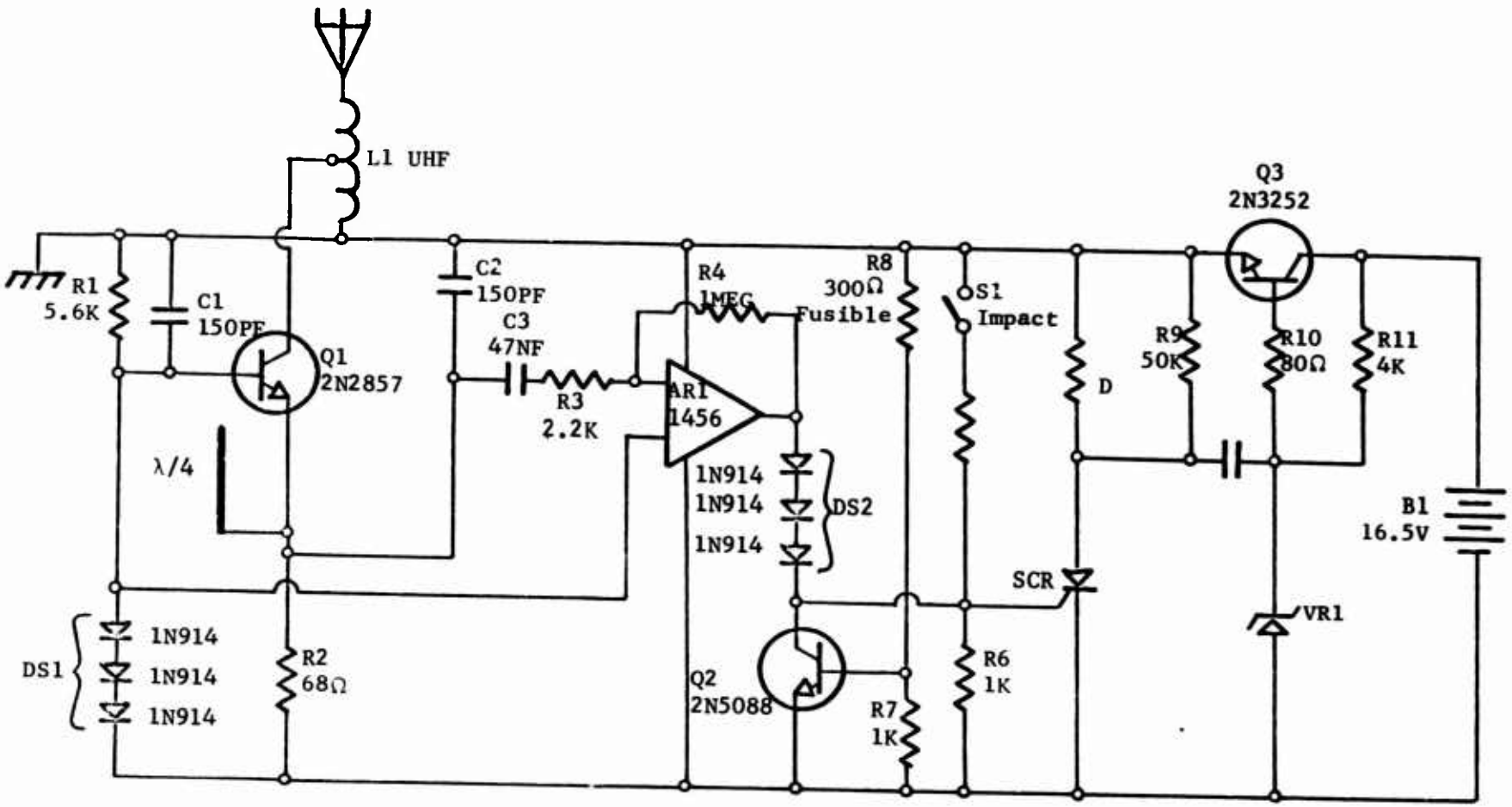

FIGURE 2. SCHEMATIC DIAGRAM OF RF PROXIMITY FUZE

supply. Thus, the voltage of sufficient magnitude is received at the inverting input and is amplified; the output exceeds 2.1 V (which corresponds to the sum of the voltage drops across the three diodes, DS2) and turns on the silicon controlled rectifier (SCR), which permits current through the detonator. The SCR can also be turned on with the closing of the impact switch, S1.

The voltage regulator consists of one transistor, Q_3, its biasing resistors R_{10} and R_{11}, and the Zener diode, VR1. Resistor R_9 and capacitor C_4 were used for detection of detonator firing during tests and are not a part of the fuze circuit. The voltage regulator maintains a constant operating voltage for the circuit. The time delay portion of the circuit consists of R_8, the fusible resistor, transistor Q_2, and resistor R_7. A time delay was needed previously since the battery became active immediately after shell firing and the fuze circuit could fire the detonator in the vicinity of its point of origin. The time delay served to keep the fuze circuit in an unarmed state. This was performed through the use of R_8 and Q_2. Current in R_8 turned on Q_2 and kept it in a saturated state, thus holding the voltage to the gate of the SCR near zero. The fusible resistor burned out after approximately 50 msec and required 300mw. After R_8 open circuited, Q_2 turned off, and the SCR could be fired by the operational amplifier.

It was determined[3] that the voltage output of the voltage regulator was approximately 10 volts, the oscillator frequency was in the region of 500 Mhz, and the minimum oscillator power output was 1-3mw. The detonator firing requirements were obtained from the manufacturer and are plotted in Figure 3.

Since this circuit had been designed for operation with a battery, several changes were needed to make it operate with a thermoelectric power source.

2. DESCRIPTION OF MODIFIED PROXIMITY FUZE CIRCUIT

The proximity fuze circuit needed to be modified to have lower power requirements and yet meet the specified performance requirements. The first item to be removed was the fusiable resistor. In the previous design, the fuzible

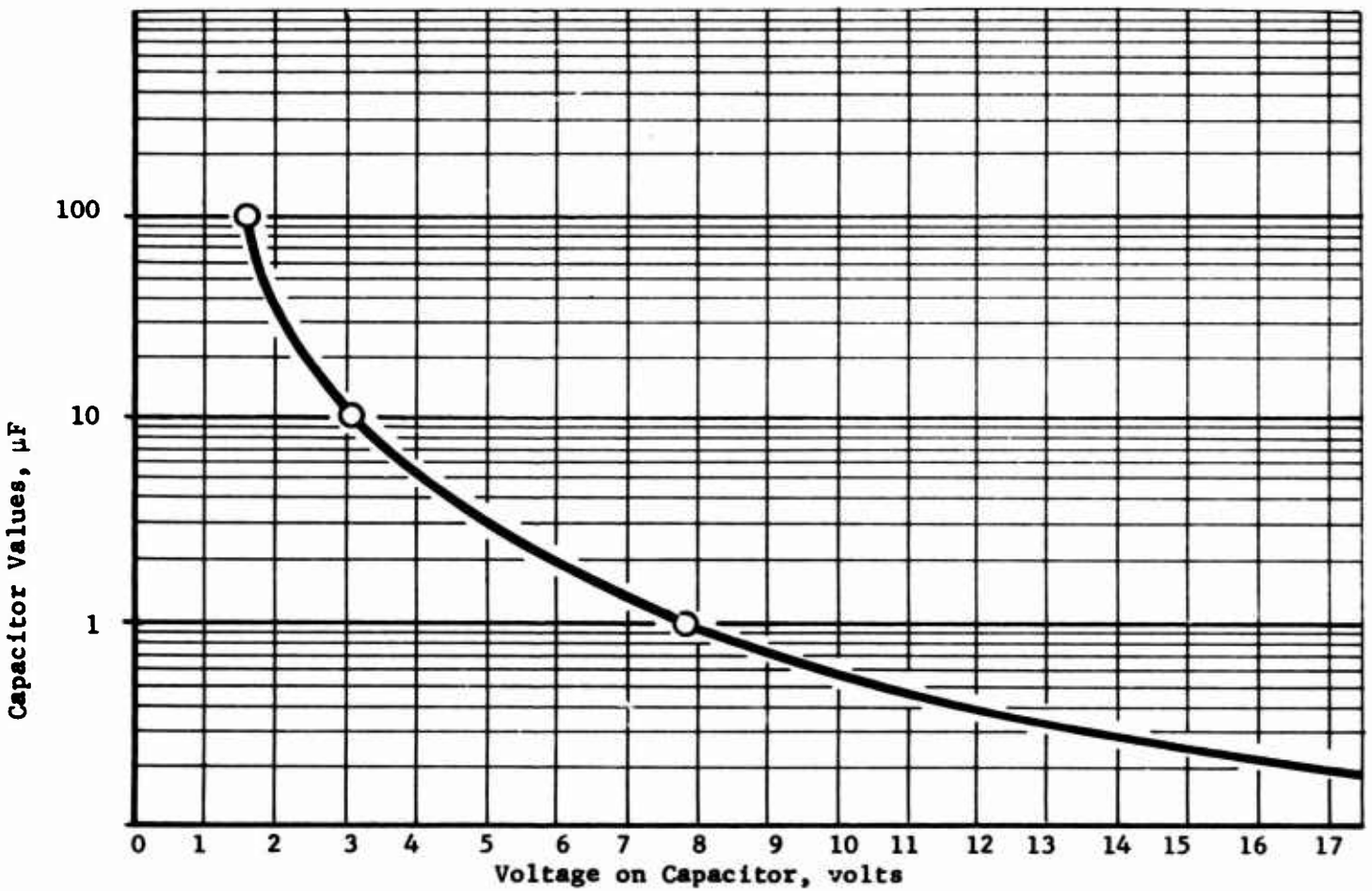

FIGURE 3. DETONATOR FIRING REQUIREMENTS

resistor provided a delay in the arming of the proximity fuze to provide a safe arming distance. In the case of the thermoelectric powered fuze, the time delay would occur naturally due to the aerodynamic heating effects and the thermal inertia of the thermoelectric elements. Also, a storage capacitor was added to supply the current necessary to activate the detonator.

The minimum voltage for the circuit is 6 volts. This lower limit is based on the threshold voltage of the operational amplifier. Thus an operating voltage of approximately 7.5 volts was chosen for this study. The power requirements at this voltage would be in the range of 40 to 50mw. Based on these considerations, the proximity fuze circuit was revised and is shown in Figure 4.

The voltage regulator limits the applied voltage to 7.5 volts. The oscillator circuit was not modified since it had been optimized in the earlier study. Diodes, D_1, were added to provide the transient to insure oscillator starting since the thermoelectric generator is a slowly rising voltage source.

It must be remembered that the revised circuit is a preliminary design and has been neither built nor tested. Therefore, the numbers given for power requirements are best estimates based on present available information. One could expect some changes in design in going from such a theoretical paper design to actual hardware and as the thermoelectric power source becomes better characterized.

3. FUZE CIRCUIT POWER REQUIREMENTS

The original circuit, Figure 2, was designed to operate at 10 volts. The operational amplifier used is a low power integrated circuit and consumes 4mw; the oscillator, 130mw, and the voltage regulator, 96mw, giving a total of 230mw. No energy storing capacitor was needed to fire the detonator because the power supply was capable of delivering the necessary current (greater than 10ma). Thus, this circuit at its operating voltage point is not compatible with a thermoelectric power source.

The revised circuit shown in Figure 4 was analyzed to determine the power requirements at 7.5 volts, the lowest voltage at which the circuit will operate. The analysis was also performed at a nominal voltage of 11 volts (see Figure 5). Analysis of this circuit was based on the requirement for an oscillator power

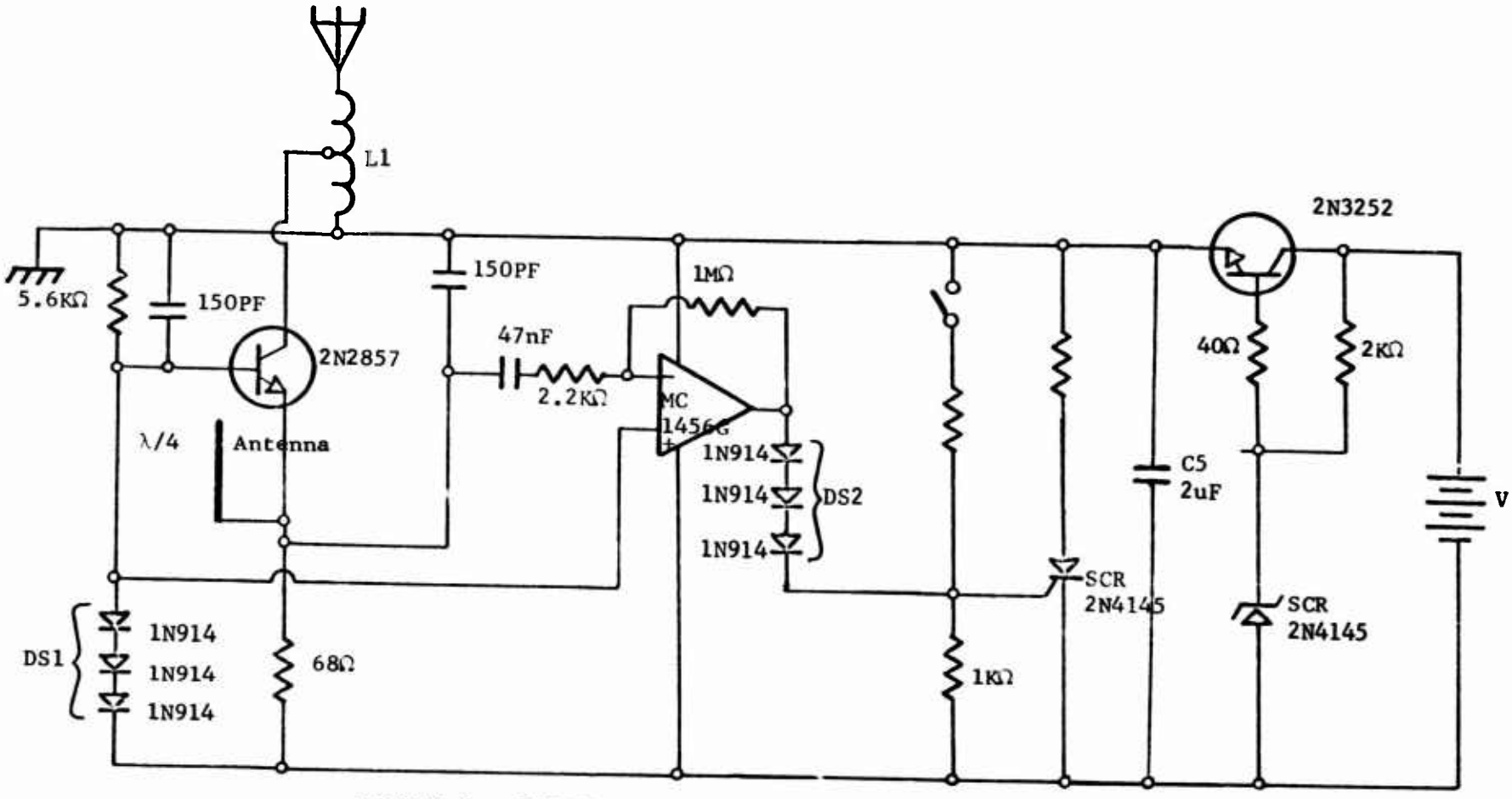

FIGURE 4. REVISED FUZE CIRCUIT (SUPPLY VOLTAGE, 7V)

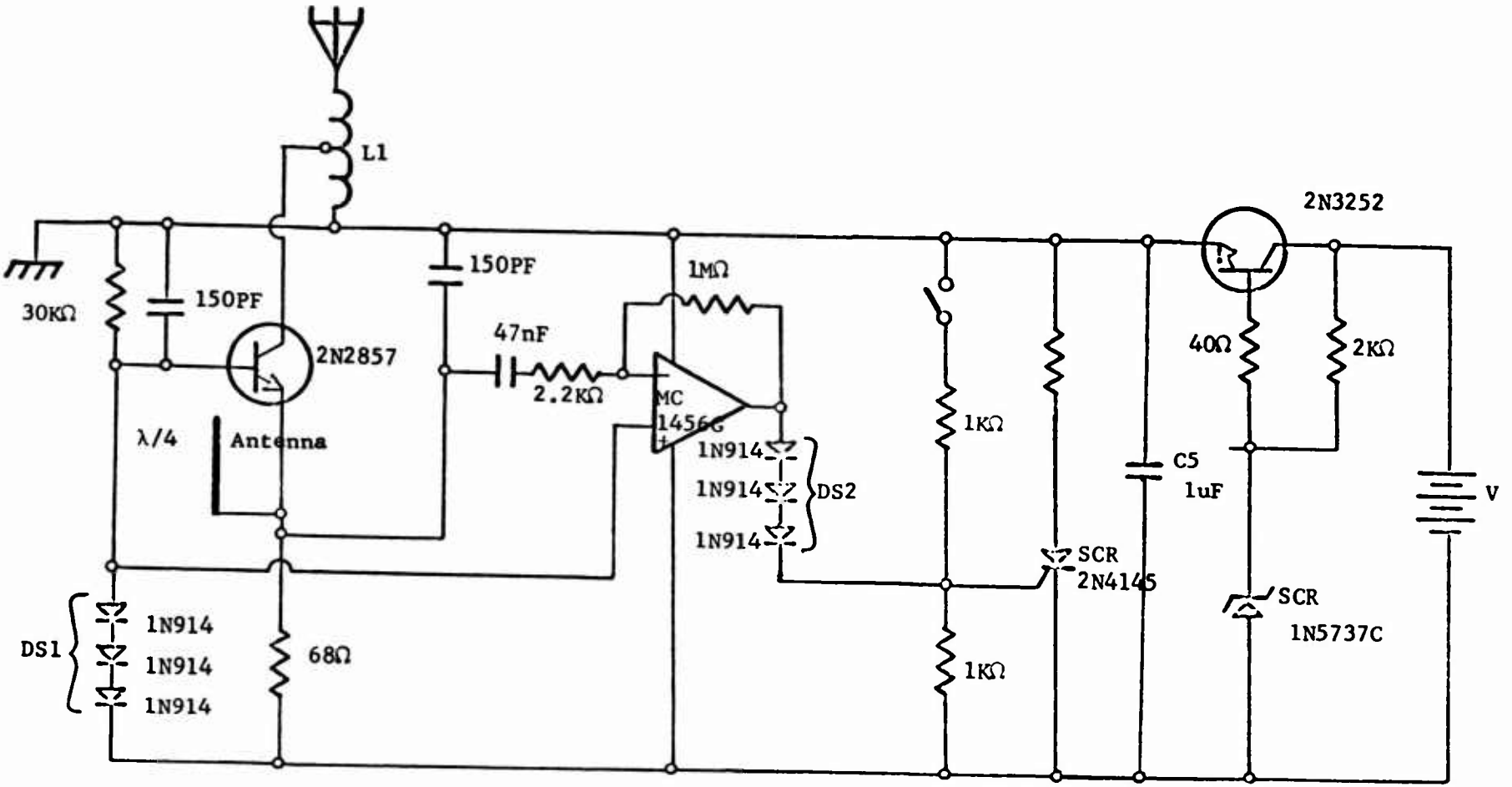

FIGURE 5. FUSE CIRCUIT (SUPPLY VOLTAGE, 11 V)

output of 1-3mw and on the assumptions of the efficiencies of the oscillator and the coupling to the transmitter antenna. The oscillator circuitry was not altered because of the previous effort[2] expended in optimizing the oscillator design. The voltage regulator was retained because the thermoelectric power supply will characteristically change with elapsed time since firing.
The study revealed that the lowest voltage at which the fuze circuit will operate is six volts. This lower limit is due to the voltage supply required by the operational amplifier. Due to tolerance variations in Zener diodes and the voltage drop across Q_3, a minimum supply voltage of 7.5 volts will be needed. The power requirements at this lowest voltage are: oscillator, 35mw; operational amplifier, 2mw; voltage regulator, 7mw; giving a total of 45mw.
The oscillator is estimated to generate a signal with a power of 4-6mw. Since neither the frequency nor oscillator efficiency was available, this approximation becomes necessary.

SECTION III

IDENTIFICATION OF CANDIDATE THERMOPILE CONFIGURATION AND ASSOCIATED MATERIALS

Based on the fuze circuit power requirements identified in the previous section of this report, a preliminary thermoelectric analysis was performed. The thermoelectric analysis was performed parametrically with respect to choice of thermoelectric material, length of thermoelectric elements, and hot-junction temperature. The results of the preliminary thermoelectric analyses are summarized in Table I and indicate

- Number of thermoelectric couples required for selected temperature difference across thermopile
- Cross-sectional area of thermoelements corresponding to selected temperature differences and thermopile configuration
- Number of thermopile units or modules required to meet fuze voltage and current requirements.

1. SELECTION OF RANGE FOR PARAMETERS

The selection of each of the parameters summarized in Table I was based on the estimated practical limits of materials properties, fabricability, and dimensional control. The rationale underlying the selection of the range for each parameter is briefly summarized below.

a. Thermoelectric Materials

There are five general classes of materials that exhibit thermoelectric characteristics: metals, semimetals, semiconductors, semiinsulators, and insulators. The metals are too low in Seebeck coefficient while too high in thermal conductivity to be of practical significance. In contrast the semiinsulators and insulators, while high in Seebeck coefficient, are too high in electrical resistivity. Of these five classes of materials, only the semiconductors and semimetals are suitable for the present energy conversion application. Within the semiconductor class,

TABLE I.
SUMMARY OF THERMOELECTRIC CONVERTER CHARACTERISTICS FOR SELECTED SEMICONDUCTOR AND SEMIMETAL MATERIALS

Thermoelectric Material	Temperature Difference,+ K	Length, L, cm	Cross Sectional Area, cm^2		Thickness of "Film", cm	Width of Couple,* cm	No. of Couples Required for 7 Volts**	No. of Couples per Disc	No. of Discs Required
			N leg	P leg					
A. Semiconductors									
Bismuth Telluride	100 K	0.254	2.52×10^{-4}	1.82×10^{-4}	2.54×10^{-3}	0.181	366	28	13
	100 K	0.508	5.05×10^{-4}	3.65×10^{-4}	2.54×10^{-3}	0.362	366	14	26
	200 K	0.254	1.98×10^{-4}	1.09×10^{-4}	2.54×10^{-3}	0.131	170	36	5
	200 K	0.508	2.87×10^{-4}	2.19×10^{-4}	2.54×10^{-3}	0.262	170	18	10
Lead Telluride	200 K	0.254	1.76×10^{-4}	2.04×10^{-4}	2.54×10^{-3}	0.160	211	30	7
	200 K	0.508	3.52×10^{-4}	4.08×10^{-4}	2.54×10^{-3}	0.320	211	15	14
Silicon Germanium	200 K	0.254	1.68×10^{-4}	1.10×10^{-4}	2.54×10^{-3}	0.115	194	40	5
	200 K	0.508	3.36×10^{-4}	2.20×10^{-4}	2.54×10^{-3}	0.230	194	20	10
B. Semimetals									
Chromel-P/Alumel	100 K	0.254	0.364×10^{-4}	0.89×10^{-4}	2.54×10^{-3}	0.050	3391	96	35
	100 K	0.508	0.729×10^{-4}	1.79×10^{-4}	2.54×10^{-3}	0.100	3391	48	70
	200 K	0.254	0.23×10^{-4}	0.533×10^{-4}	2.54×10^{-3}	0.040	1689	120	14
	200 K	0.508	0.46×10^{-4}	1.066×10^{-4}	2.54×10^{-3}	0.080	1689	60	28
Chromel-P/Constantan	200 K	0.254	0.204×10^{-4}	0.364×10^{-4}	2.54×10^{-3}	0.033	1041	144	8
	200 K	0.508	0.408×10^{-4}	0.728×10^{-4}	2.54×10^{-3}	0.066	1041	72	15

* Assume 0.005 cm gap between adjacent elements.

** Assume zero contact resistivity for these preliminary analyses.

\+ Cold junction temperature = 300 K in all cases.

those materials offering the highest energy conversion efficiency include bismuth telluride, lead telluride, and silicon germanium. Chromel-P/Alumel and Chromel-P/Constantan combinations are representative of the semimetal class of materials.

b. Temperature Difference

The selection of the range of temperature differences between the hot-junction and cold-junction of the thermopile was based on the minimum required temperature difference for practical-sized thermopiles and the maximum anticipated temperature difference based on the available aerodynamic heating rates.

c. Thermoelement Length

The upper limit of the range selected for this parameter was determined by the overall dimensions of the projectile. The lower limit on the thermoelement length is influenced by the practical limits of the proportionately smaller cross-sectional area of the thermoelements as well as the increasing proportion of power dissipated at the thermoelement/electrode junctions. In addition, at decreasing thermoelement lengths, hence cross-sectional areas, the thermal heat flux requirements will exceed the available aerodynamic heat flux.

d. Thickness of Thermoelements

Based on the preliminary thermoelectric analyses using the averaged-parameter technique, [4] it was apparent that the cross-sectional dimensions of the individual thermoelements (for all materials considered) were beyond the limits of cost-effective fabrication by the "discrete element" approach. One alternative fabrication method involves the vapor deposition of a thin film of the thermoelement on an appropriate substrate. For the purposes of the present comparative analysis, film thicknesses of 0.00254 cm (0.001 in.) and 0.00508 cm (0.002 in.) have been selected.

2. SELECTION OF THERMOPILE CONFIGURATION

With the range for thermopile design parameters established, the next step was to identify a feasible thermopile configuration. In order to provide the required substrate surface area, a concept featuring the use of a multiplicity of disc-

shaped modules (see Figure 6) has been evolved. In this scheme, a series arrangement of thermoelements is deposited on both sides of the disc-shaped substrate. This overall module design scheme was used in the comparative thermoelectric analyses discussed next. The physical location of the disc modules in the projectile tip is shown in Figure 7.

3. SELECTION OF CANDIDATE THERMOPILE DESIGN

The results of the comparative thermoelectric analysis summarized in Table 1 indicate that the bismuth telluride thermopile features a number of advantages including

- Fewest number of couples required
- Fewest number of disc-shaped modules required
- Lowest heat flux requirement
- Practical element width from standpoint of physical masking.

The semimetals are attractive from the standpoint of a simpler materials system (no dopant required) and a lower base cost for the materials. However, the thermopiles involving semimetals involve very small thermoelement widths, thus complicating the vapor deposition process and associated masking requirements.

This analysis indicates that bismuth telluride is the most promising thermoelectric material for the present 20-mm projectile power supply requirements. Based on these results, more detailed analysis of the overall thermopile performance was performed and is reported in Section V.

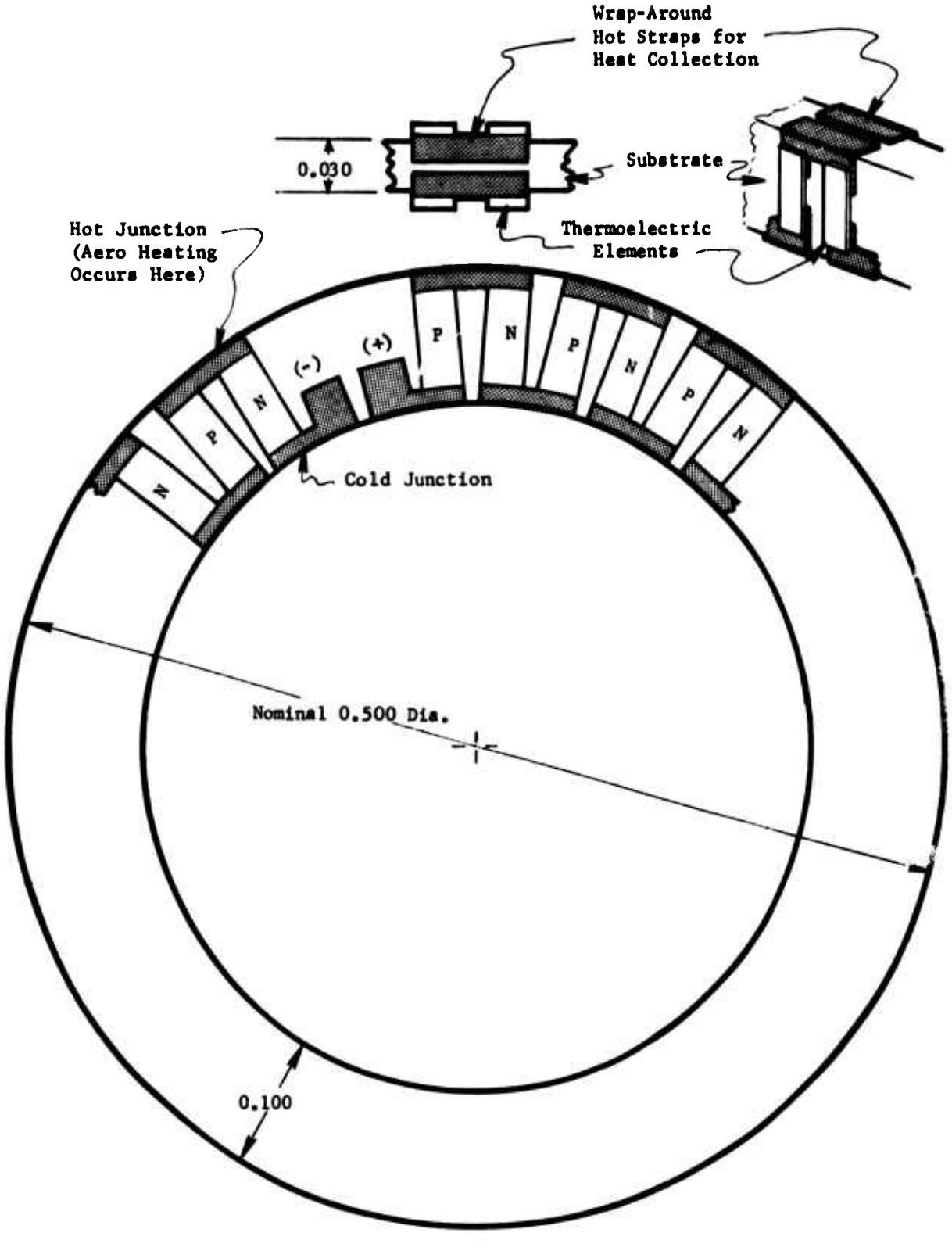

Note: All Units in Inches

FIGURE 6. DISC-SHAPED THERMOELECTRIC MODULE CONCEPT FEATURING THIN-FILM THERMOELEMENTS

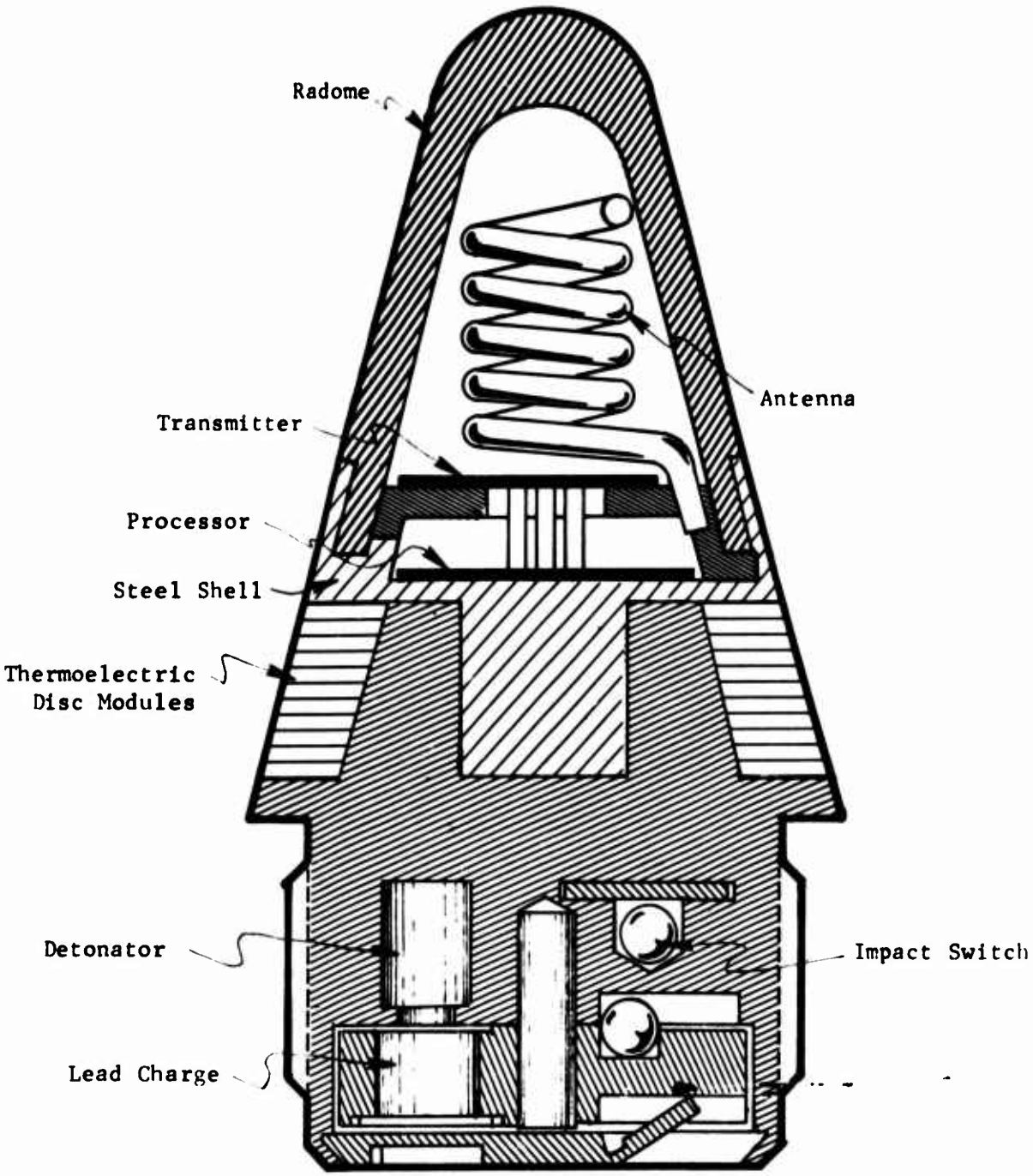

FIGURE 7. CROSS-SECTIONAL VIEW OF 20 mm PROJECTILE INVOLVING DISC THERMOELECTRIC MODULES

SECTION IV

AERODYNAMIC HEATING ANALYSIS

The objective of the aerodynamic heating analysis is to establish the maximum and minimum surface heating rates experienced by a typical 20 mm projectile. Aircraft altitude and velocity are to be included as variables, and the heating rates are to be determined as a function of position along the projectile surface. The results of the analysis will be used as input to the thermopile design optimization.

1. BLUNT CONE CONFIGURATION

The blunt cone configuration, typical of a 20 mm projectile shown in Figure 8, produces a rather complex flow field. The curvature of the bow shock wave generated by the blunt nose of the projectile causes the entropy to vary from streamline to streamline. Due to the growth of the boundary layer across streamlines, the fluid properties in the boundary layer vary with surface distance. This effect is propagated far back on the conical portion of the body. As a result, boundary layer heating cannot be accurately predicted by simple analytical techniques which rely, for example, on the principle of boundary layer similarity.

After examining the various available computer programs with the capability to calculate convective heating to blunt cones, the NOL RETAS code was chosen. This program has been developed over several years by personnel at the Naval Ordnance Laboratory[5,6] to compute drag and convective heating on spherically blunted cones. The projectile trajectory is computed, and drag and distributed convective heating are calculated at selected points along the trajectory. The code is ideally suited to this subtask.

2. LAMINAR BOUNDARY LAYER HEAT TRANSFER

The NOL RETAS Code utilizes the energy-integral approach to determine the Stanton number distribution along the surface of a blunted cone at zero angle-of-attack. The energy-integral approximation is similar to the Von Karman momentum-integral approach. An energy-integral equation is developed by

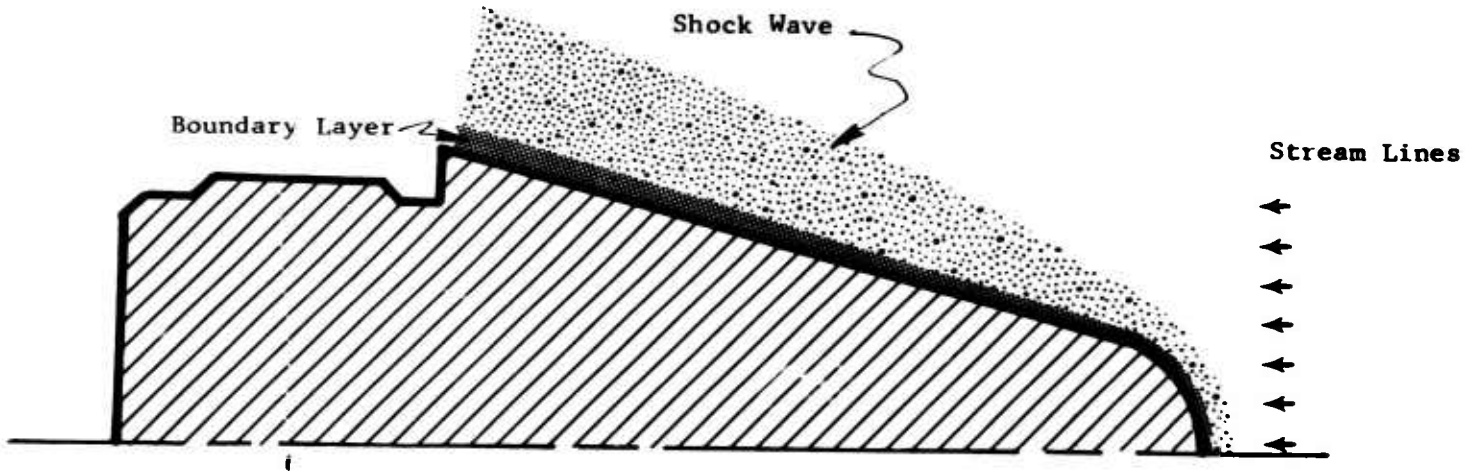

FIGURE 8. SCHEMATIC OF BLUNT CONE FLOW FIELD TYPICAL OF 20mm PROJECTILE

integrating the energy equation through the boundary layer. The resulting equation is then solved by using a reference temperature method and an incompressible, flat-plate Stanton number relation. The solution assumes perfect gas flow over the cone. Complete details of this method are given in References 5 and 6.

Once the boundary layer properties are determined, the local skin friction coefficient and the heat-transfer rate are found. The skin friction coefficient is integrated over the body and contributes to the total drag calculation. The local heat transfer rate is given by

$$q_w = \rho_1 U_1 C_p (T_1^* - T_w)\ St$$

where St is the Stanton number, ρ_1 and U_1 are the boundary layer edge density and velocity, respectively, T_w is the wall temperature, and T_1^* is the reference temperature.

The surface heat transfer rates calculated in this manner have been compared with the blunt cone measurements of Reference 7. The results are presented in Figure 9 as

$$\frac{N_u}{R_e} = \frac{q_w/K(T_1^* - T_w)}{R_e}$$

versus s/r_n*. The calculations compare very well with the data on the conical part of the body.

3. PROJECTILE SPIN EFFECTS

The high rate of spin of a typical 20 mm projectile produces magnus forces and moments which are important to the flight dynamics of the projectile. It is also possible that the spinning of a projectile will influence the character of the boundary layer so that boundary layer heating will be affected.

The first order effect of spin can be estimated by comparing the true surface velocity, including spin, with the projectile axial velocity. The true surface velocity is obtained by vectorially adding the axial and tangential velocities of the surface. For an axial velocity (muzzle velocity) of 4000 ft/sec and a projectile spin of 120,000 rpm, the true surface velocity is

---

* s/r_n refers to distance along projectile surface(s) from the stagnation point divided by the nose radius, r_n.

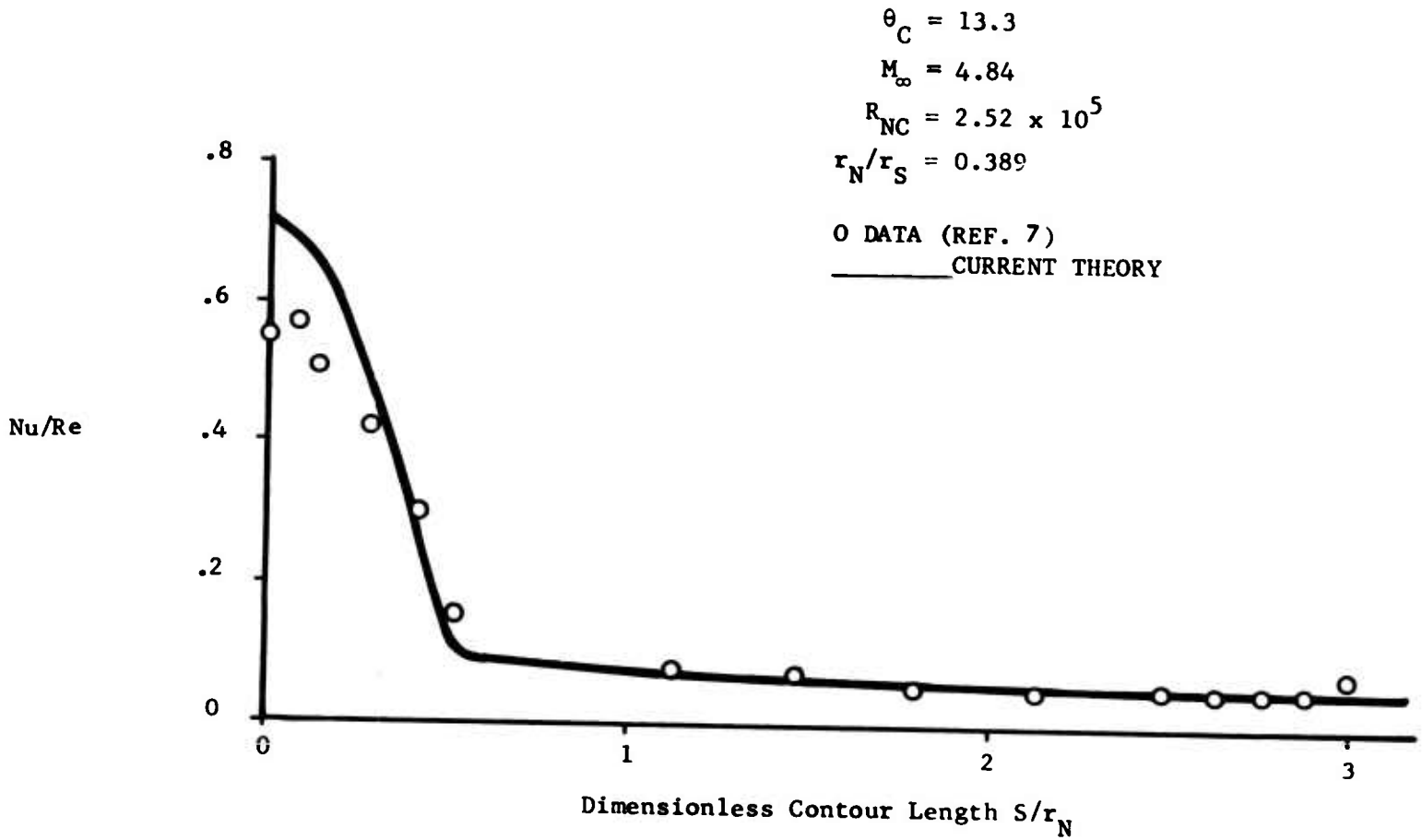

FIGURE 9. COMPARISON OF EXPERIMENTAL DATA WITH THEORY FOR LAMINAR FLOW OVER A BLUNTED CONE, REF 1

$$V_s = V_{axial}^2 + \frac{\omega d}{2}^2 = 4020 \text{ ft/sec},$$

where ω is the projectile angular velocity and d is the projectile diameter, which is within 1/2% of the axial velocity. Thus, as a first order influence, projectile spin can be neglected.

Evidence supporting this conclusion is reported in Reference 8. In Reference 8, pitot pressure surveys were made of the laminar boundary layer on an ogive-cylinder model, at Mach 3.02 and 4.10. Boundary layer properties were compared between zero spin and a spin rate relative to axial velocity of twice that for the 20 mm projectile discussed above. The data confirm the earlier conclusion that the zero angle-of-attack boundary layer velocity profiles do not appear to be affected significantly by model spin.

4. BOUNDARY LAYER TRANSITION

The blunt cone configuration is generally used for supersonic and hypersonic projectiles because it is an optimum shape with regard to low drag projectiles. Blunting a sharp cone effectively reduces drag in two ways. First, the bow shock wave produced by the blunt nose significantly reduces the flow velocity along the cone boundary layer edge below the value that would exist on a sharp cone. This reduces the skin friction drag (as well as boundary layer heating), which is the major contributor to the total projectile drag. Secondly, blunting a cone has been shown to inhibit boundary layer transition from laminar to turbulent flow. A turbulent boundary layer can produce 3 or 4 times the skin friction of a laminar boundary layer.

The reason nose blunting forstalls transition is still uncertain and will not be discussed here. There is, however, a great deal of boundary layer transition data for blunt cones, for both free flight and wind tunnel experiments. Tetrevin[9] has developed a correlation parameter, based on theoretical considerations, which successfully correlates the results from 48 ballistic range tests for cones. Tetrevin's correlation predicts transition at a length Reynolds number of

$$Re_x = 0.226 \times 10^5 \; G_t^{0.7764}$$

where

$$G_T = \frac{T_w}{T_e}^{2/3} \left[1/2(T_w/T_e+1) + 0.0037\, M_e^2\right]^{4/3} Re_\phi .$$

The data and correlation are presented in Figure 10. The results are reasonably well described by the correlation. This correlation has been used to predict the occurrance of transition or lack of transition and the subsequent effect on aerodynamic heating for the 20 mm projectiles analyzed during this program.

5. RESULTS OF BOUNDARY LAYER HEATING CALCULATIONS

The range of parameters over which the convective heating to 20 mm projectiles must be considered is presented in Figure 11. Shown on the altitude-Mach number map is the range in these parameters a projectile might experience upon being fired from a F-111, a helicoptor, and from the rear of a B-52. Superimposed on the map are curves of constant convective heating rate. Also, a curve of constant Reynolds number, equal to 20×10^6, is given. To the right of this line it is possible that transition to turbulent boundary layer flow will occur on parts of the projectile.

As an example of the results obtained from analyses of the convective heating rates on the 20 mm projectile, detailed calculations for the nominal case (indicated by a * in Figure 11) are presented in Figures 12 and 13. A 0.20-lb projectile, fired at 3500 ft/sec from 3000 ft at an angle of -20 degrees from the horizontal, was considered for the nominal case. The projectile range and velocity history are shown in Figure 12. In Figure 13, the distributed convective heating to the projectile surface is presented at three times during the first second of flight. The heat transfer rate is seen to drop off dramatically in this first second due to the decrease in projectile velocity. At some time the projectile velocity will be so low that the projectile will experience cooling by the free stream instead of heating.

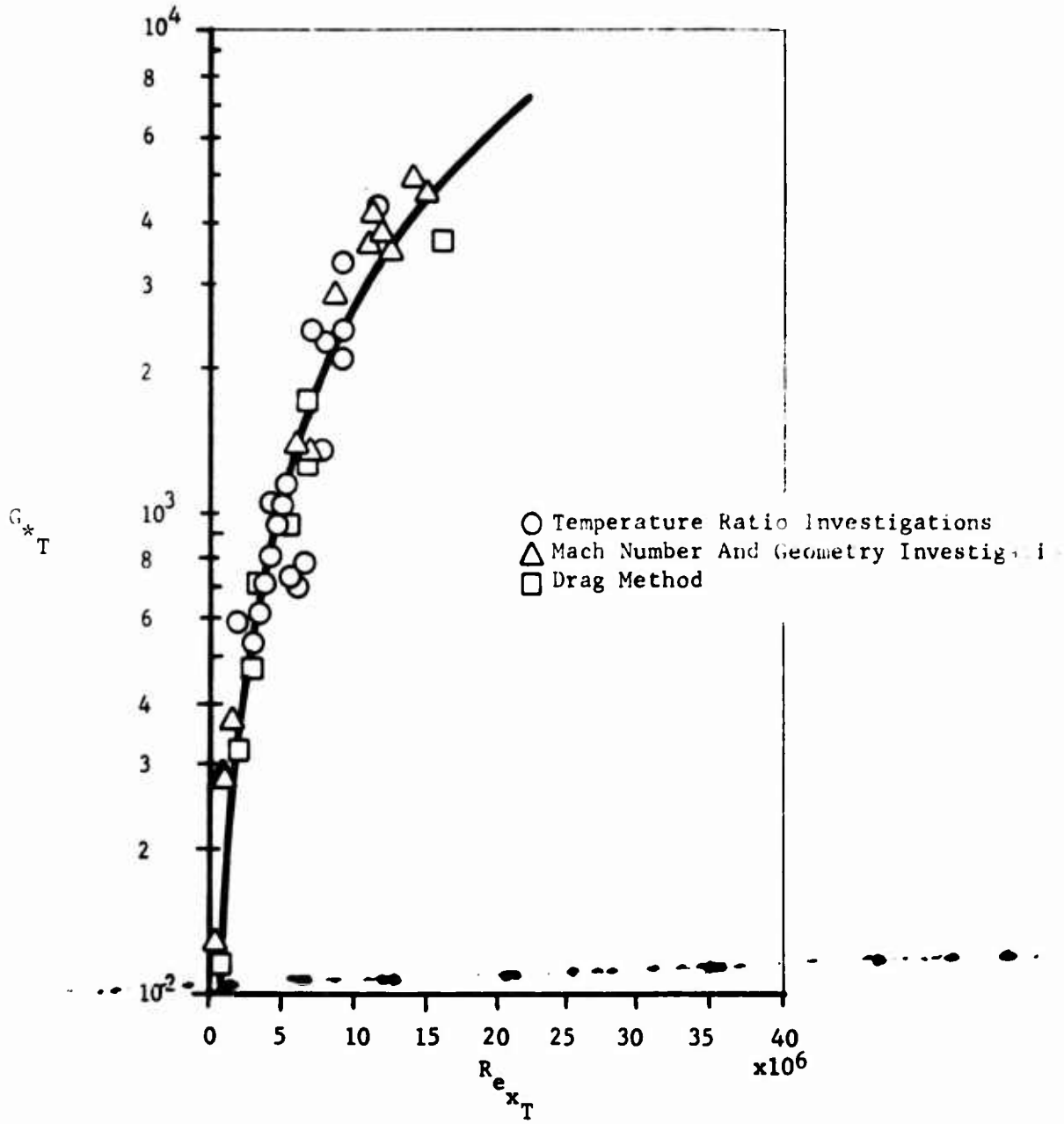

FIGURE 10. COMPARISON OF TRANSITION CORRELATION WITH DATA FOR BALLISTICS RANGE

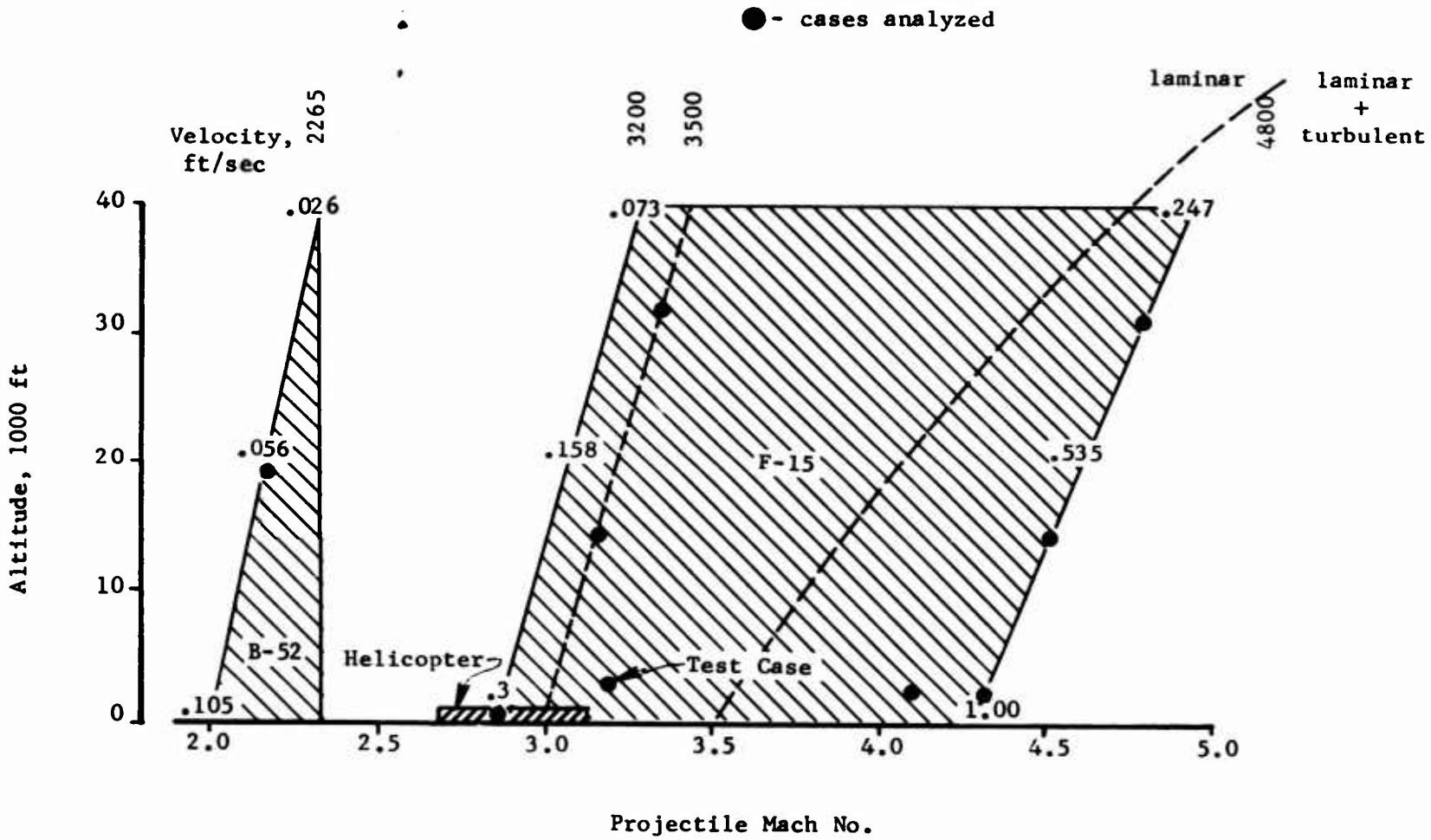

FIGURE 11. ALTITUDE-MACH NO. MAP FOR 20mm PROJECTILE FIRED FROM VARIOUS VEHICLES

20 mm Projectile Heating

Range and Velocity History

Projectile Weight = 0.20 lb

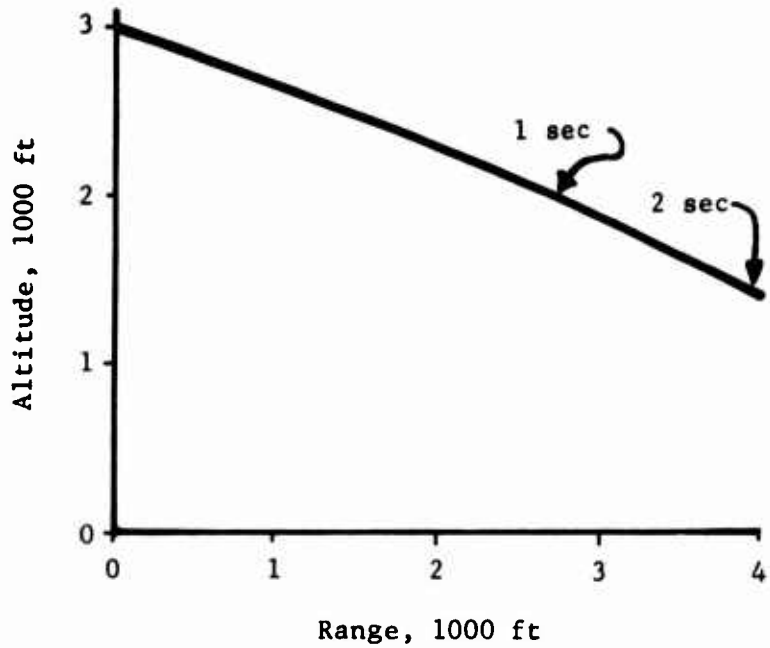

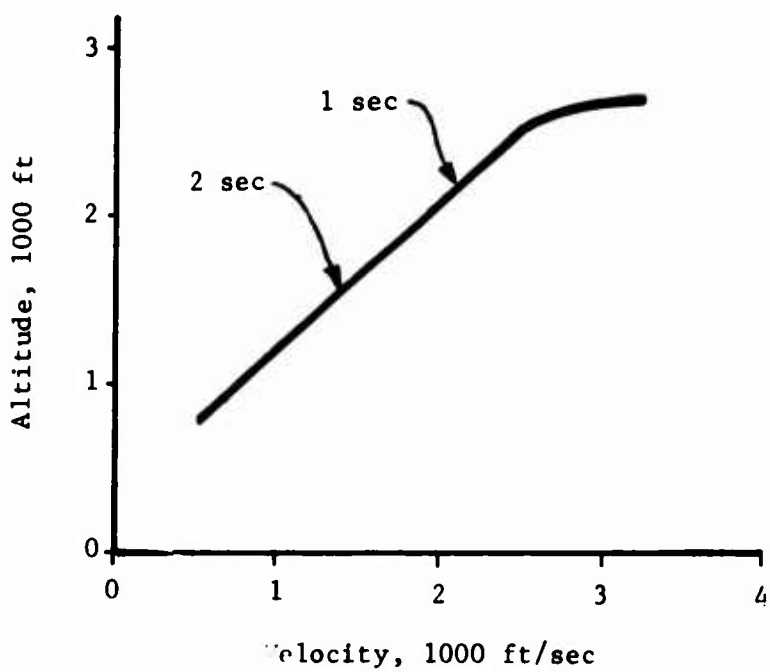

FIGURE 12. RESULTS OF TRAJECTORY CALCULATION FROM RETAS CODE

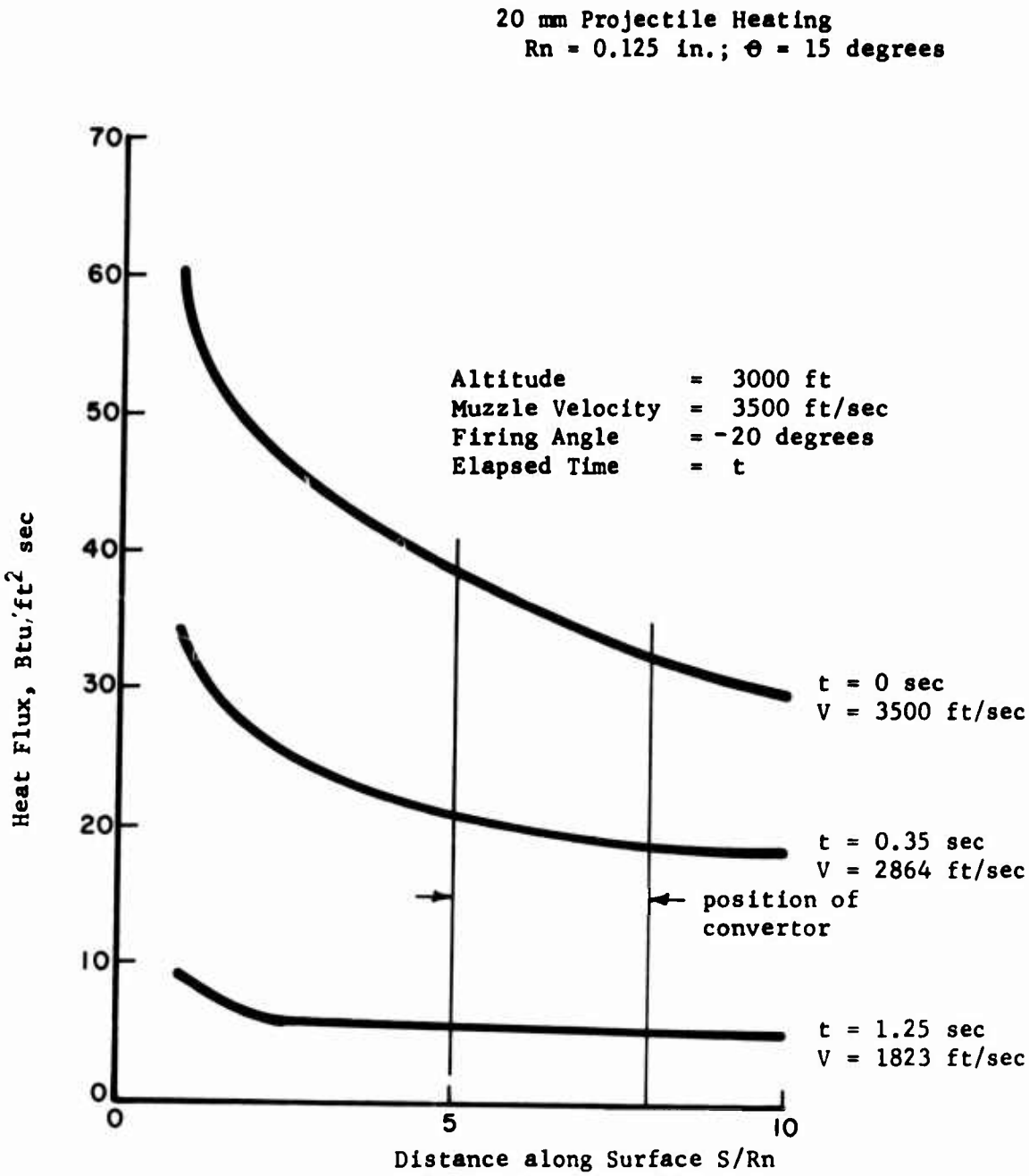

FIGURE 13. DISTRIBUTED HEATING ON 20 MM PROJECTILE

Calculations (see Figure 14) of heat transfer rates were performed for the 20-mm projectile at representative points throughout the map of Figure 4. It was found that laminar boundary layer flow prevailed except at one small region of the F-111 range. Transition occurred near the base of the cone ($s/r_n = 13$) at speeds greater than Mach 4 and altitudes of 3000 ft and less. However, in all cases relaminarization occurred as the projectile slowed down, such that by $t = 0.2$ sec the flow was completely laminar.

The aerodynamic heating rate for a 30-mm projectile is included in Figure 14 and illustrates the effect of a larger projectile mass on the velocity decay rate, hence, aerodynamic heating rate. The performance of thermoelectric convertor for a 30-mm projectile will be included in a later section of this report along with selected cases involving 20-mm projectiles.

Substantiation of the absence of transition on the cone of a 20-mm projectile is found in Reference 10. In Reference 10 the temperature history of various components of a 20-mm projectile was obtained by transient heating tests in a Mach 5 blowdown tunnel. It was found that turbulent flow existed on the shell casing, downstream from the cone, at a Reynolds number per foot of 20×10^6. Below this Reynolds number, laminar flow existed on the entire shell. Since it would require a slightly higher value of Reynolds number to move transition onto the cone, it is felt that the results of Reference 10 are in agreement with the transition criteria used in this study.

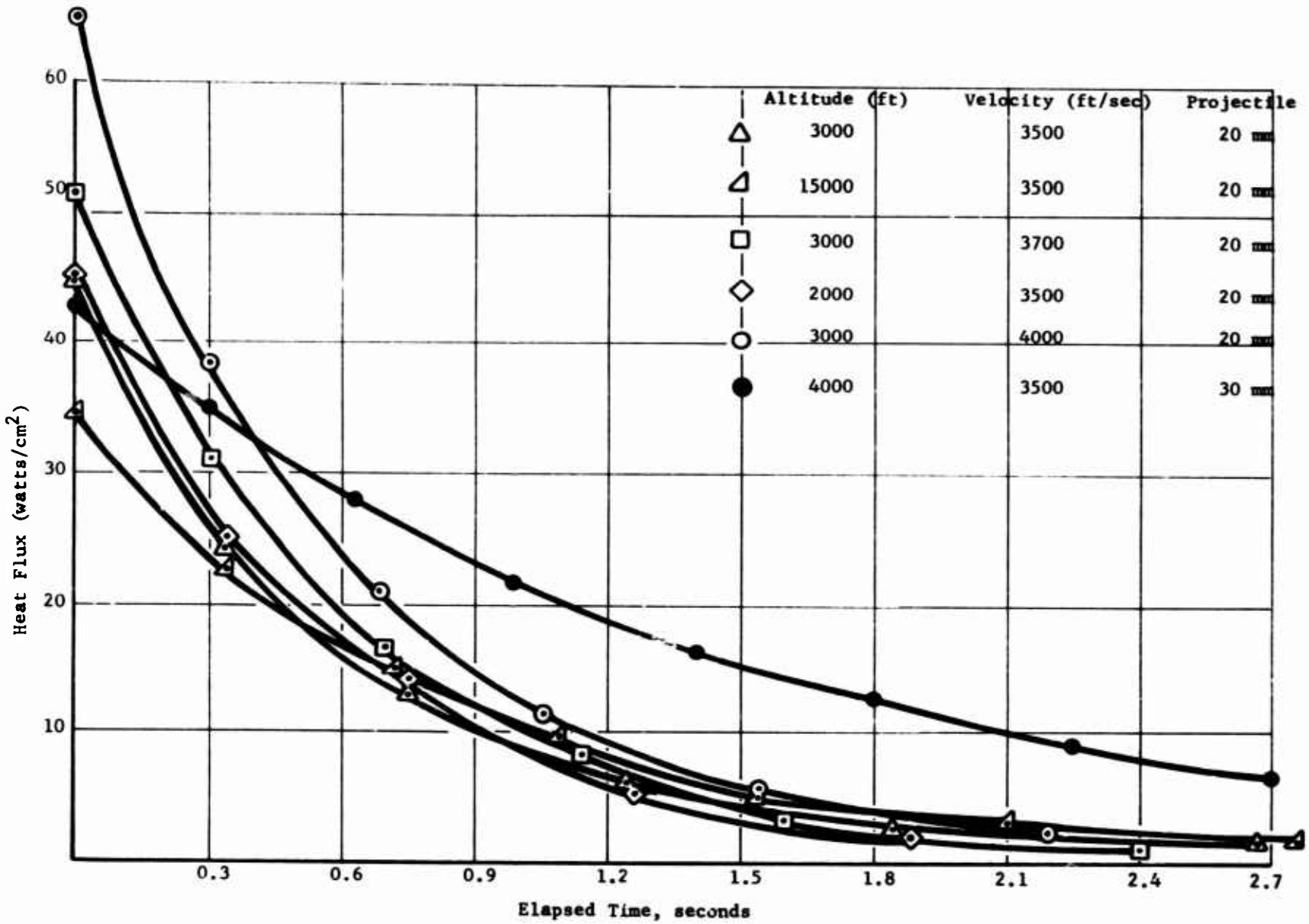

FIGURE 14. AERODYNAMIC HEATING OF THE PROJECTILE AT A POINT 1.3 cm FROM TIP FOR A FIRING ANGLE OF -20 DEGREES

SECTION V

OPTIMIZATION OF THERMOPILE DESIGN

The results of the thermopile materials/design study discussed in Section III were were translated into a thermal model for the purpose of transient thermal analysis of the thermopile under simulated conditions of firing. The thermal model for the disc thermoelectric module configuration is shown in Figure 15. The dimensions, thermal connections, and properties associated with the network of nodes (subregions) shown in Figure 15 provide the input data for the TRUMP * heat transfer computer program.

The input data for this thermal analysis include:

- Dimensions of each subregion
- Thermal conductivity, specific heat, density associated with each material in the system
- Heat transfer coefficients associated with internal and external interfaces
- View factors and surface emittances at internal and external interfaces
- Surface heat flux as a function of time
- Initial temperature of subregions.

The output data provided by the thermal analysis include

- Temperature of each subregion as a function of time
- Heat transferred in and out of each subregion.

The calculated temperature profile of the thermoelectric converter as a function of time provides the basis for estimating the output power of the thermoelectric converter as a function of time. These analytical results thus provide the rationale for such design tradeoffs as increasing (decreasing) the "thermal storage" capability of the disc converter and introducing electrical power storage for the latter phase of the trajectory.

---

* See Appendix for description of TRUMP computer program.

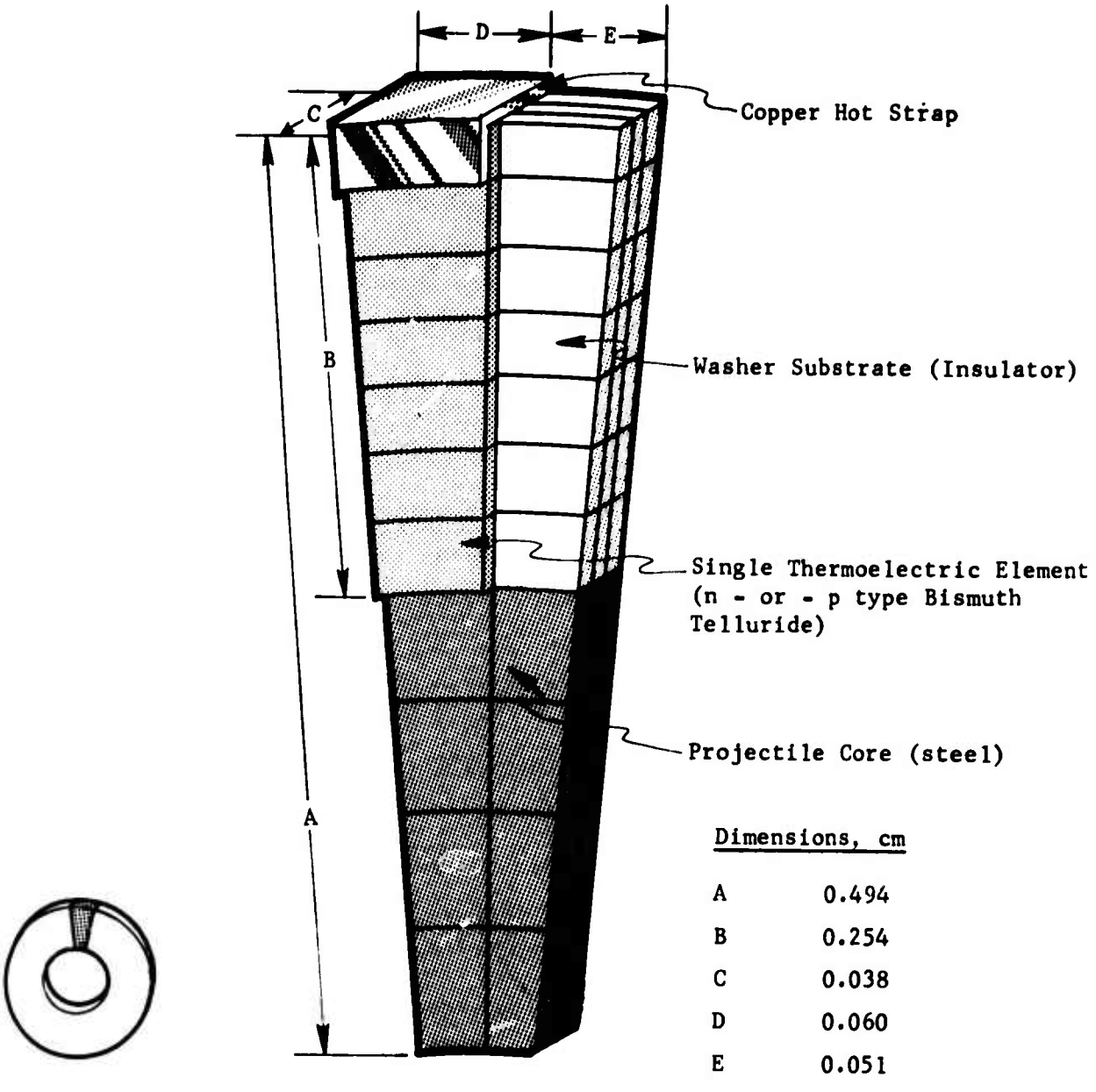

FIGURE 15. THERMAL MODEL OF DISC THERMOELECTRIC CONVERTER CONCEPT

1. DESCRIPTION OF THERMAL MODEL

The thermal model for the thermoelectric disc converter is illustrated in Figure 15. The first step in the development of the thermal model involved partitioning the disc module into the smallest sector of symmetry with respect to the temperature profile of the disc module. In the present case, the smallest sector of symmetry involved one-half of the disc thickness with an angular sector which includes one thermoelectric element plus the region between two adjacent thermoelectric elements (see Figure 15). Once the smallest sector of symmetry was identified, the next step involved subdividing this sector of the disc into subregions. These subregions were interconnected by equivalent "thermal resistances" based on the temperature-dependent thermal conductivity of the materials involved, the dimensions of the subregions, and the interface thermal impedances (if any) between two given subregions. The heat capacitance of each subregion was obtained from the product of the subregion volume and the temperature-dependent specific heat of the material occupying that subregion.

The assigned thermal capacitances and thermal coupling between subregions thus comprise the thermal model used in the present study. The parameters for the thermal analysis of the connector included

- Substrate material
- Time-dependent aerodynamic heating rate (simulating various altitude/muzzle velocity combinations)
- Hot strap thickness.

The constants and property data used in this thermal analysis included

- Bismuth Telluride thermoelectric element ($\bar{k}$ = 0.0162 watts/cm-C, C_p =0.0107cal/g)
- Steel projectile core ($\bar{k}$ = 0.512 watts/cm.C, C_p = 0.460cal/g)
- Thermal impedance at the core/disc interface = 0 $(watts/cm^2.C)^{-1}$
- Thermal impedance at all other interfaces = 0$(watts/cm^2.C)^{-1}$
- Dimensions as shown in Figure 15.

In this model, 0.005 cm thick copper hot straps (see Figure 6) were included in order to improve the transfer of aerodynamic heat from the outer surface of the disc to the thermoelectric element. As shown in Figure 6, the copper hot strap was positioned over the outer face of the disc and extended or "wrapped" over the side of the disc and in thermal/electrical contact with the thermoelectric element.

2. THERMAL ANALYSIS OF DISC CONVERTER FOR SELECTED SUBSTRATE MATERIALS

The next step in the optimization of the thermoelectric converter design involved identifying preferred substrate (disc) material(s). The criteria for selecting substrate materials included

- Low thermal conductivity
- Capability of operation at temperatures up to 400 F (205 C)
- High tensile strength.

In these analyses only the reference case was considered, i.e., 20 mm projectile fired at 3000 foot altitude with a muzzle velocity of 3500 ft/sec. A parametric analysis involving three substrate materials (alumina, Pyroceram 9606, and Kapton) was performed. The results of this analysis are summarized in Table II and indicate that the substrate (disc) thermal conductivity must be an order of magnitude lower than the thermoelement thermal conductivity in order to develop adequate temperature differences (e.g., 50 C or more) across the thermoelements. This is particularly important when one considers that the thickness of the disc is seven times larger than the thermoelectric elements.

With identification that the disc converter design involving Kapton allowed adequate temperature differences to develop across the thermoelements, additional parametric analyses were performed to evaluate temperature difference across the converter and corresponding output power as a function of time for selected time-dependent aerodynamic heating rates. These results are discussed next.

TABLE II.
COMPARISON OF PEAK TEMPERATURE DIFFERENCES ACROSS THERMOELEMENTS FOR SELECTED SUBSTRATE MATERIALS

Substrate Material	Thermal Conductivity, Watts/cm-C		Peak Temperature Difference, K
	Substrate	Thermoelement	
Alumina	0.28	0.016	10
Pyroceram 9606	0.037	0.016	34
Kapton	0.002	0.016	105

3. TEMPERATURE DIFFERENCE ACROSS CONVERTER AS A FUNCTION OF TIME

A total of nine cases were next analyzed to determine the temperature difference developed across the thermoelements as a function of time for selected altitudes and muzzle velocities. The cases analyzed are summarized in Figure 11 in terms of aircraft altitude and projectile Mach number. The results of these analyses are summarized in Figure 16 and indicate that significant temperature differences can be achieved in all but the low muzzle velocity case. This case corresponds to the rear-firing guns on a B-52 aircraft. The results were next used to estimate the thermoelectric couple output power as a function of time under matched load conditions.

4. OUTPUT POWER AS A FUNCTION OF TIME

Of the nine cases considered above, five were further analyzed to determine the couple open-circuit voltage and output power as functions of time. This analysis was performed as illustrated below for each leg of the thermocouple:

$$\text{Open circuit voltage, } V_{oc} = \sum_{i=i}^{7} S_i(T)\ \delta T_i$$

$$\text{Internal resistance, } R_{int} = \frac{L}{A} \sum_{i=i}^{7} \rho_i(T)$$

$$\text{Output power*, } P = \frac{(V_{oc})^2}{4\ R_{int}}$$

The summation is taken over the seven segments which make up the overall thermoelement (see Figure 14).

The results of these analyses are summarized in Figures 17 and 18 and indicate that an adequate output power per couple should be produced by aerodynamic heating for elapsed times of one second or more. Note that at the higher

---

* Matched load conditions.

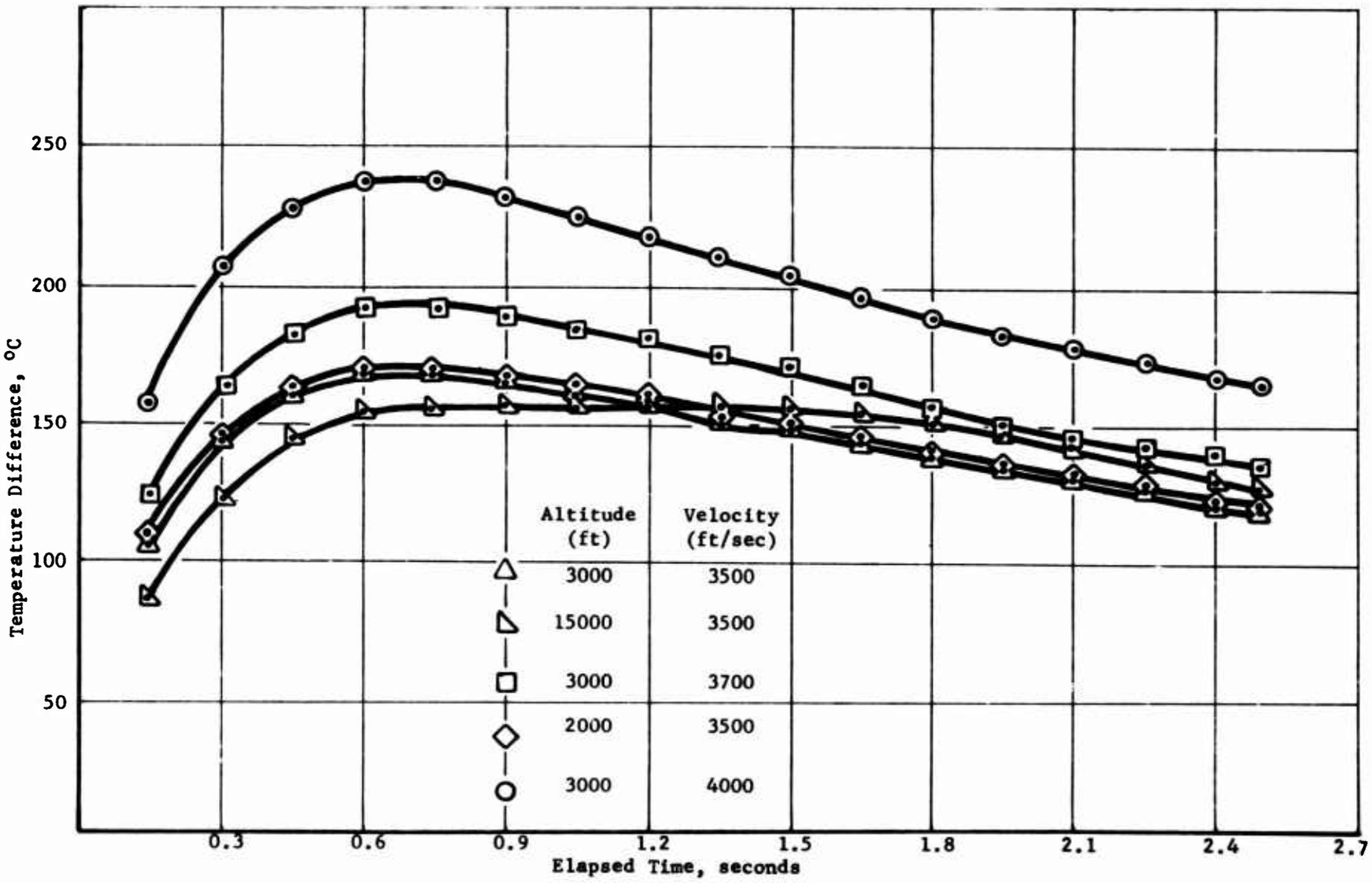

FIGURE 16. TEMPERATURE DIFFERENCE ACROSS CONVERTOR AS A FUNCTION OF TIME

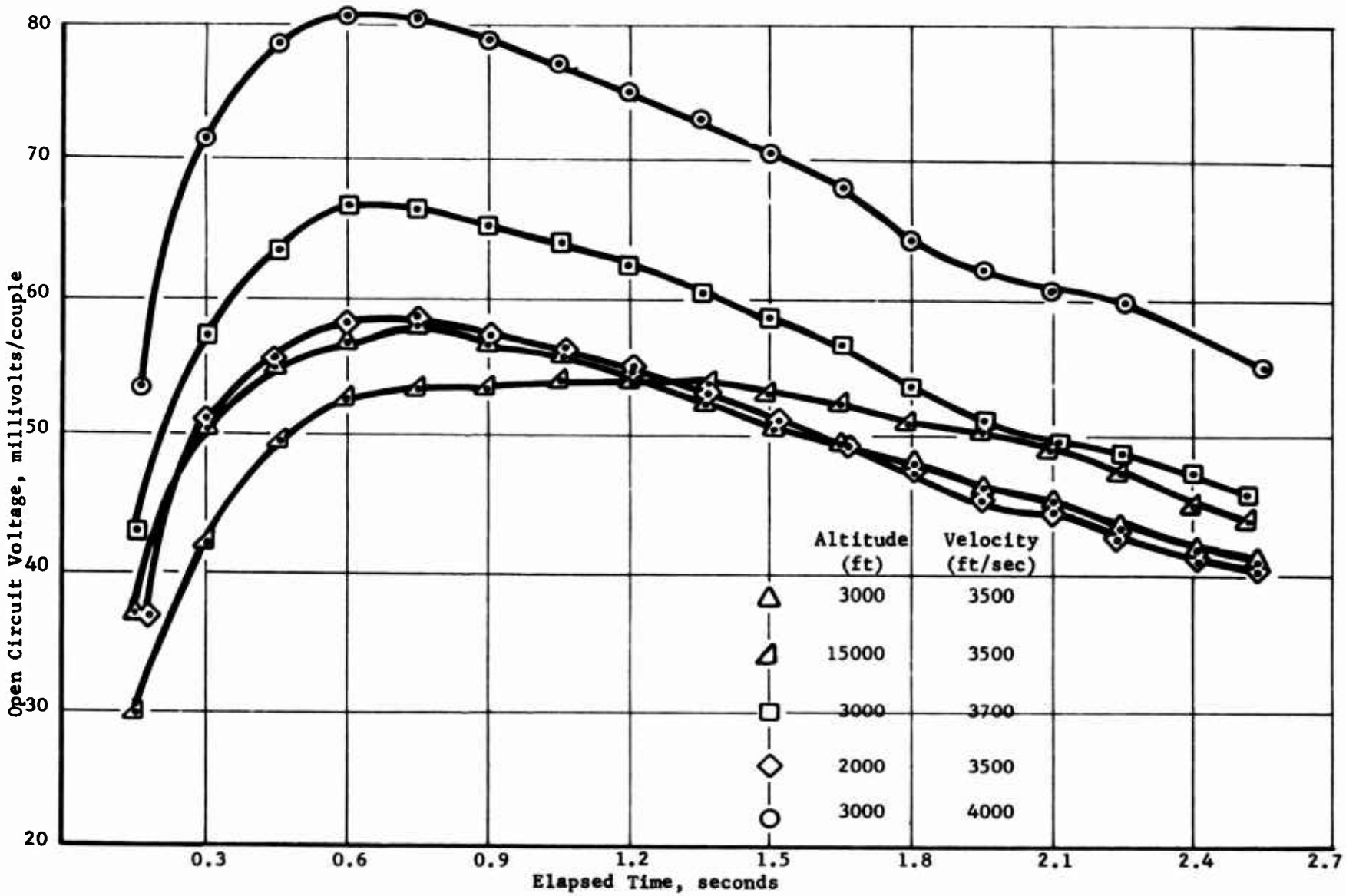

FIGURE 17. CONVERTOR OPEN CIRCUIT VOLTAGE AS A FUNCTION OF TIME

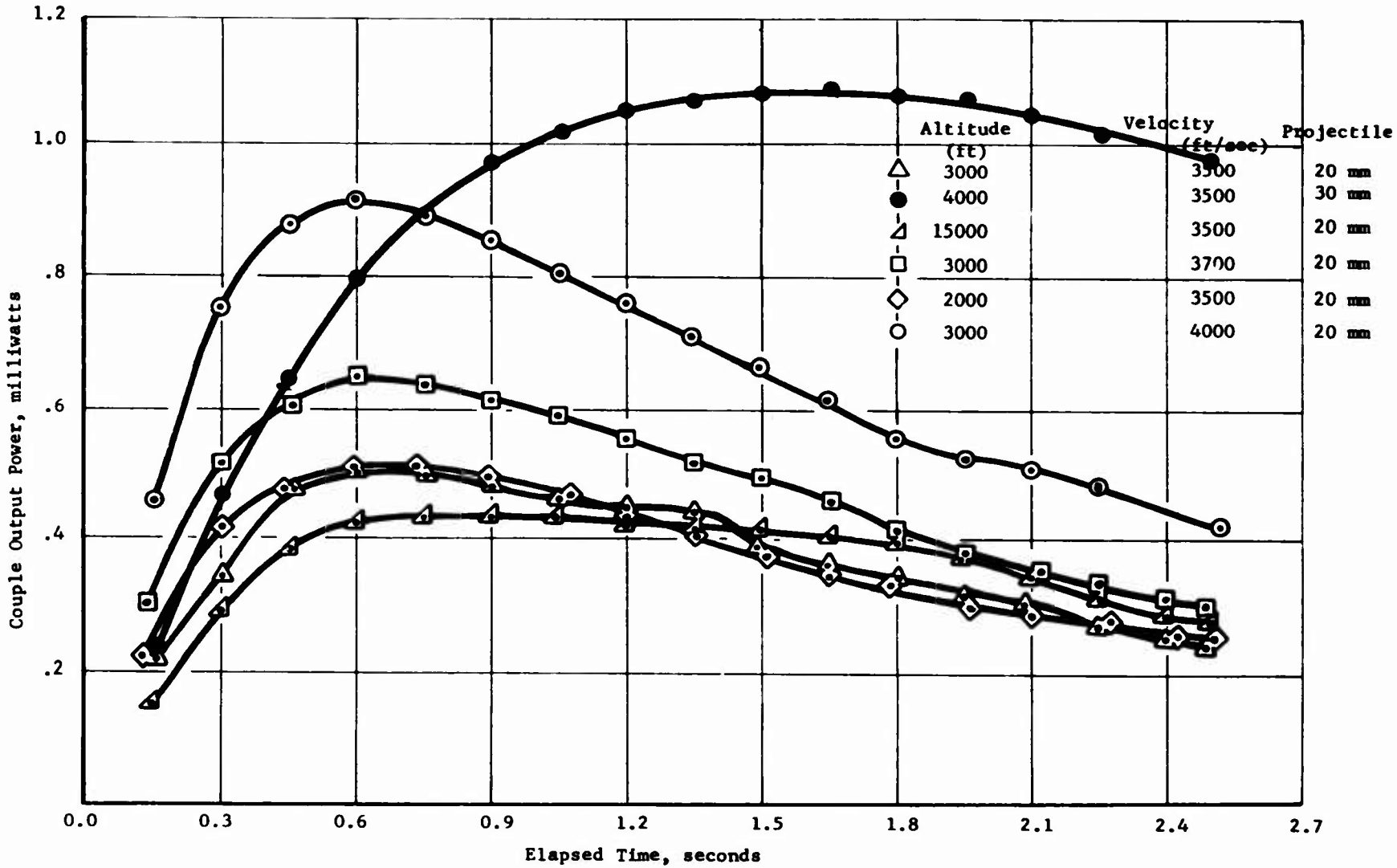

FIGURE 18. CONVERTOR OUTPUT POWER AS A FUNCTION OF TIME

velocity (4000 ft/sec) a significantly larger output power owing to the high aerodynamic heating rates is generated. Clearly, for higher muzzle velocities, there is some incentive to produce excess electrical power during the early period of the trajectory and store it for use in the later periods when velocity and, hence, output power have decayed substantially.

Without energy storage, the number of couples required to produce 40 milliwatts output power is inversely proportional to the minimum couple output power encountered during the trajectory lifetime. This relationship is illustrated in Figure 18 and indicates that, for 3000 feet altitude and 3500 ft/sec muzzle velocity, the number of couples required for a trajectory lifetime of 2.5 second is approximately 220. However, with suitable energy storage, this couple requirement might be reduced to 150 couples. The options for energy storage will be discussed later in this section.

5. SENSITIVITY OF THERMOPILE TEMPERATURE DIFFERENCE AND OUTPUT POWER TO MUZZLE VELOCITY

Additional aerodynamic heating analyses were performed to provide projectile surface heating rates as a function of muzzle velocity and elapsed time after firing. In these analyses, the altitude (3000 feet) and firing angle (-20 degrees) were maintained constant for muzzle velocities ranging from 3500 to 4800 ft/sec. The purpose of this limited parametric analysis was to estimate the sensitivity of the aerodynamic heating rate and temperature difference to the projectile muzzle velocity over the period of the projectile trajectory. Accordingly, the sensitivity of the related temperature difference across the thermopile can be translated to the open circuit voltage and output power as a function of muzzle velocity. The results of this sensitivity analysis thus provided the basis for translating 20 mm projectile muzzle velocity distributions into thermopile output power and peak hot-junction temperature distributions.

The results of this parametric analysis are summarized in Table III and indicate that the temperature difference, ΔT, and output power (per couple), P, are related to the muzzle velocity, V, as follows (after elapsed time of 0.3 second):

$$\Delta(TH - TC) = 0.1565\ (\Delta V)\ (3500 \leq V \leq 4800)$$

$$\Delta P = 0.0012\ (\Delta V)$$

P = output power in milliwatts

TC, TH = temperatures in C

V = velocity in ft/sec.

A review of a reported muzzle velocity uniformity study[11] revealed that 20 mm ammunition based on M246 IED test firings in a XM163 automatic cannon can be characterized by a muzzle velocity of 3380 ± 50 ft/sec. Based on the above findings, this 2.7 percent change in velocity would correspond to a couple output power variation (after elapsed time of 0.3 second) of approximately 22 percent.

The above results can now be translated into operational requirements for aircraft deploying the subject 20 mm projectiles. Specifically, the range of aircraft speed suitable for use with aerodynamically heated thermoelectric (bismuth telluride) power supplies can be estimated by assuming a nominal muzzle velocity of 3380 ft/sec based on a stationary aircraft cannon. The results summarized in Table III indicate that a minimum effective muzzle velocity (muzzle velocity plus aircraft speed) of 3500 ft/sec is required in order to provide adequate output power up to at least a 2.5 second trajectory (for no energy storage). At the other extreme, the maximum effective muzzle velocity is 4500 ft/sec to avoid exceeding the upper operating temperature limit of the disc thermoelectric converter. These two extremes translate to maximum and minimum aircraft speeds of 1120 ft/sec (760 mph) and 120 ft/sec (80 mph), respectively, at a firing altitude of 3000 feet.

6. SENSITIVITY OF THERMOPILE TEMPERATURE DIFFERENCE AND OUTPUT POWER TO ALTITUDE AT FIRING

At higher altitudes, the upper and lower limit aircraft speeds will be reduced due to the lower aerodynamic heating rates encountered in the less dense air which lead to a delayed, but larger, temperature difference. For example,

TABLE III.
VARIATION IN TEMPERATURE DIFFERENCE AND OUTPUT POWER AS A FUNCTION OF MUZZLE VELOCITY[a] FOR 20-MM PROJECTILE

Elapsed Time Since Firing, seconds	Effective Muzzle Velocity, feet/second					
	3500		3700		4000	
	ΔT[b]	P[c]	ΔT	P	ΔT	P
0.3	146	0.339	167	0.511	208	0.752
0.6	167	0.499	194	0.647	236	0.912
0.9	166	0.483	189	0.612	231	0.850
1.2	159	0.441	181	0.552	219	0.758
1.5	149	0.384	170	0.482	205	0.665
1.8	139	0.336	156	0.406	187	0.552
2.1	130	0.293	144	0.346	178	0.495
2.5	119	0.245	133	0.296	162	0.411

(a) Based on an altitude of 3000 feet and firing angle of -20 degrees.

(b) Temperature difference across thermoelectric convertor in centigrade degrees.

(c) Electrical output power per couple in milliwatts.

compare the thermopile temperature difference as a function of time since firing, shown in Figure 16, for two cases--15000 ft and 3000 ft altitude at 3500 ft/sec effective muzzle velocity. The lower altitude (3000 ft) case illustrates the effect of the increased aerodynamic drag in the denser air--resulting in an early peak in the temperature difference (see Figure 16) followed by a steep decay in the temperature difference during the remainder of the trajectory. In contrast, the high altitude (15000 ft) case reflects a lower aerodynamic drag--resulting in a relatively slow increase in the temperature difference across the thermopile during the first 1.0 second of the trajectory (see Figure 16).

It is interesting to note that, from the above comparison of thermopile performance for low and high altitudes, the use of energy storage (to extend the useful range of the projectile) is effective only at lower firing altitudes. At these lower altitudes, excess power is produced during the early period of the trajectory whereas at higher altitudes the major fraction of the power produced occurs later in the trajectory.

7. CIRCUIT ANALYSIS OF FUZE CIRCUIT POWERED BY THERMOELECTRIC CONVERTER

To examine the performance of the fuze circuit with the thermoelectric generator, the fuze circuit was analyzed with the computer program, SCEPTRE*. SCEPTRE is a circuit analysis program capable of determining the transient and steady state responses of large electrical networks. Of particular interest were the delay times for circuit activation, power consumption during the trajectory, and detonator firing at the termination of the trajectory.

Fuze circuit operation was investigated by considering projectile firings from selected altitudes and effective muzzle velocities. The thermoelectric open-circuit voltage (as a function of elapsed time from firing) for these different conditions was used, and a total of eight situations were analyzed.

---

* Developed at Kirtland Air Force Base.

The revised circuit shown in Figure 4 was modeled for SCEPTRE analysis. An arbitrary number of 300 thermocouples was selected for the thermoelectric voltage source. The calculated thermoelectric voltage as a function of time after firing used in these analyses is given in Figure 17. The calculations were terminated at 2.5 seconds after firing, except for the low altitude case. The firing angle was maintained constant at -20 degrees from the horizontal axis for all cases considered.

Table IV illustrates the relationships among the firing parameters and the operation of the proximity fuze circuit. The time delay column indicates when the circuit becomes active after firing. The duration column indicates the elapsed time after firing that the circuit is actively sensing a target. In other words, the proximity fuze is no longer active if the thermoelectric voltage has dropped below the threshold voltage of approximately 9 volts necessary to operate the RF circuitry. However, the detonator circuitry remains armed after the RF sensor ceases to function due to the stored energy in the 2μF capacitor. The detonator is then activated upon impact through the closing of the impact switch, S1.

From Table IV it can be seen that the revised proximity fuze circuit is "compatible" with the thermoelectric voltage source. From the use of 220 couples, the length of time the proximity fuze circuit remains active is more than 2.5 seconds at muzzle velocities of 3500 ft/sec or more. This duration corresponds to an active range for the proximity fuze of more than 6000 feet.

To extend the time of operation (hence, range) for the proximity fuze circuitry, the following steps may be taken:

- Increase projectile's initial velocity
- Increase number of thermocouples
- Utilize energy storage
- Revise the circuit design.

All or any of these factors can be used to increase the active life of the circuit. From Table IV we can see that in most cases the delay time (time until activation) is satisfactory for operational conditions. However,

TABLE IV.
RELATIONSHIP OF FIRING CONDITIONS WITH PROXIMITY
FUSE CIRCUIT PERFORMANCE

Altitude (ft)	Initial Muzzle Velocity (ft/sec)	Time Delay (sec)	Duration of Active RF Circuit (sec)	No. of Thermocouples
2,000	3,500	.080	> 2.5	300
3,000	3,500	.100	> 2.5	300
15,000	3,500	.100	> 2.5	300
3,000	3,700	.080	> 2.5	300
3,000	4,000	.050	> 2.5	300

the duration of an active proximity circuit can be improved by increasing the effective muzzle velocity. For example, comparing the three initial velocity conditions at a 3000-foot altitude indicates that an initial velocity of 3700 ft/sec or greater provides a longer duration, hence, range.

Alternatively, the number of thermocouples could be increased to 366 (maximum for space available), which would provide additional voltage. The voltage would increase by a factor of 1.66.

Energy storage was also considered in extending the active life of the circuit. Initial calculations indicate a capacitance on the order of 1000 μF would be needed to supply the necessary current for 1 second. However, the space limitations associated with the present circuit design prevent the use of chip capacitors on the surface of the existing circuit boards. As an alternative, a separate substrate containing a multiplicity of chip capacitors or a discrete element capacitor might be added to the projectile tip.

Also, the RF circuit may be further modified. The circuit was not optimized since the objective was to determine if mating a proximity fuze circuit with a thermoelectric power supply was feasible. With the construction of a breadboard circuit and further computer circuit analyses, the proximity fuze circuit may be optimized to function for the different firing conditions using less than the present input power at 40 milliwatts.

8. ADVANTAGES AND LIMITATIONS OF ENERGY STORAGE IN RF PROXIMITY FUZES

The previous discussion has indicated that one method for extending the period during which the RF fuze is "active" is to use energy storage. By using storage, excess power produced by the thermoelectric converter during the early phase of the trajectory would be available to supply the needed threshhold voltage and current during the later phase of the trajectory. (For example, see Figure 18, 3000-ft altitude, 4000-ft/sec muzzle velocity.)

Based on the findings of this study, the following are requisite conditions for the effective use of energy storage with 20-mm projectiles:

- Aircraft altitude (during firing) should be below 25,000 ft.
- Effective muzzle velocity should be at least 3500 ft/sec.

Several approaches to energy storage can be considered--thermal and electrical energy storage. Thermal storage is effected through the use of thicker hot straps (see Figure 15) or surrounding the thermoelectric converter with an outer layer of metal or ceramic. For example, a 0.010 in. thick sleeve of metal (copper or aluminum) enclosing the disc modules (see Figure 7) would affect the output power versus time as shown in Figure 19.

A second possible approach to energy storage involves the storage of electrical energy. As indicated in Subsection 7, a 1000 μF capacitor would be required to extend the "active life" of the RF fuze by 1.0 second, or about 500 μF of capacitance for 0.5 second increase in active life. "Chip" capacitors which can be placed in planar substrates (consistent with the present circuit configuration) are available in capacitances up to only 2 μF. Hence, 250 to 500 of these 0.225 in. x 0.210 in. chips would be required for the present projectile. Alternatively, a discrete tubular capacitor component may be used instead but will occupy a volume of 0.5 in.^{3} to 1.0 in.^{3} for the 500 to 1000 μF capacitors, respectively. For the case of the 20-mm projectile, this volume requirement limits the use of electrical storage unless (1) the projectile tip can be enlarged or (2) the central core of the projectile is bored out to accommodate a tubular capacitor.

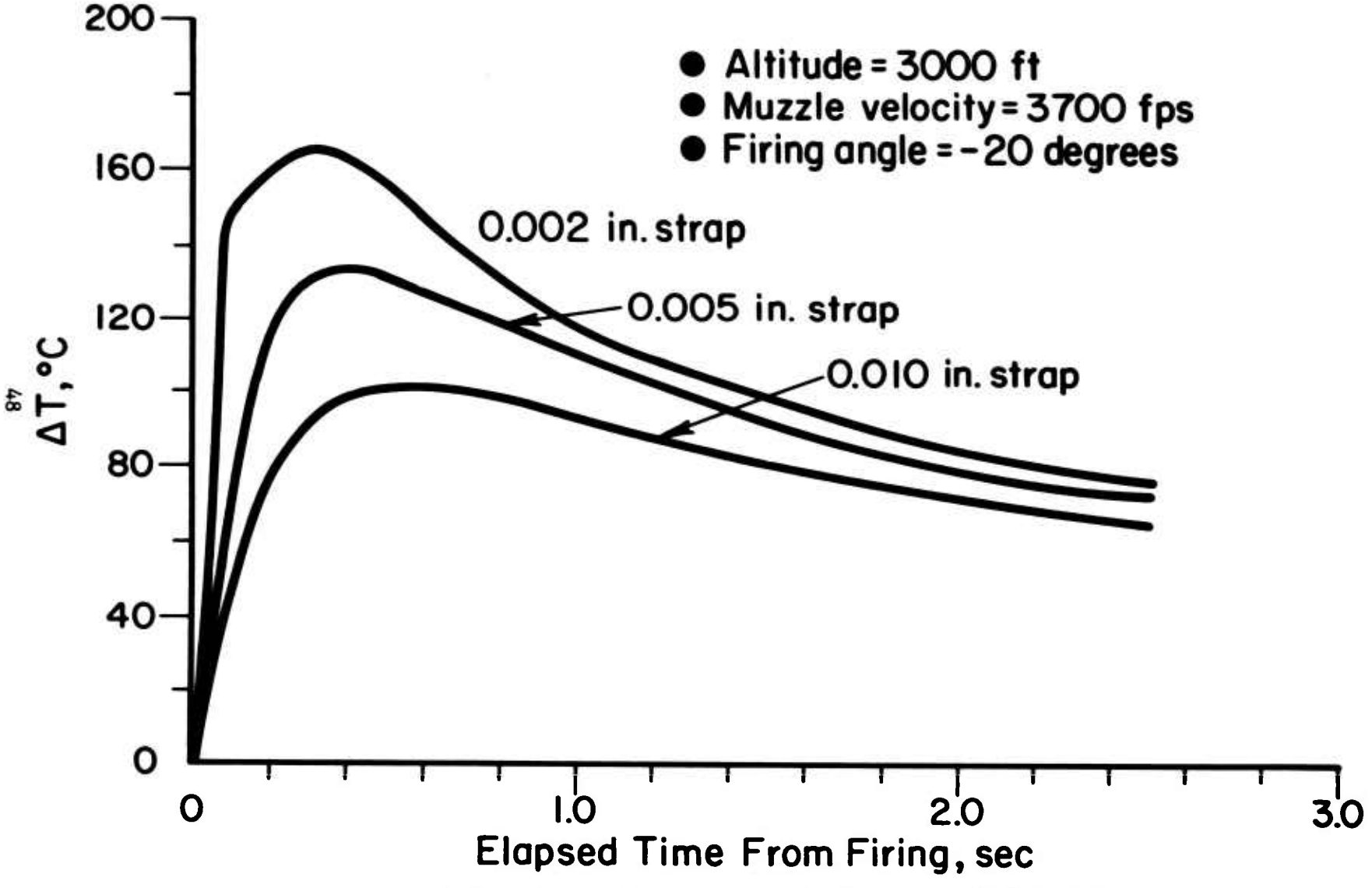

FIGURE 19. TEMPERATURE DIFFERENCE ACROSS THE THERMOELECTRIC CONVERTER FOR SELECTED HOT STRAP THICKNESSES

SECTION VI

STRUCTURAL ANALYSIS OF DISC THERMOELECTRIC CONVERTOR

A preliminary structural analysis of the projectile tip as modified for a thermocouple generator is discussed next. Since the detailed design of the projectile will not be initiated until Phase II, these efforts have considered only the overall structural integrity of the thermopile with an attempt to identify possible problem areas.

1. ANALYTICAL APPROACH

The overall dimensions and configuration of the tip are shown in Figure 7. Loadings to the tip are a spin ratio of 2000 rev/sec and a peak acceleration level of 120,000 g's. In addition, aerodynamic heating gives a (222C) temperature rise at the surface of the Vespel polyimide discs which make up the thermocouple generator. It was assumed that the impulse accelerating the projectile is such that dynamic stress wave propagation effects are negligible. The 120,000 g acceleration can then be considered a quasistatic inertia loading.

It is understood that the projectile prior to the present modification has been demonstrated to withstand the imposed loadings. Thus it is necessary only to consider the region in the area of the circumferential groove in which the thermoelectric convertor is positioned. The following properties were used for the polyimide substrate in the structural analysis:

Elastic Modules = 4.8×10^5 lb/in.^{2},

Density = 0.046 lb/in.^{3},

Strength = 10,000 psi,

Thermal Expansion Coefficient = 2.85×10^{-5} in./in./F. = α

It was recognized that the polyimide material has an elastic modulus about 50 times less than that of the adjacent steel components. Thus it was reasonable to assume that loads from the projectile tip will be transferred entirely through the steel shell, and not through the plastic discs. Also it was assumed that the steel shell can be treated as rigid relative to the polyimide.

2. ROTATIONAL STRESSES

Although the discs will probably be bonded or mechanically fixed into the groove of the steel body, in the stress analysis no credit was taken for support of the disc by the body. Thus rotational stresses were calculated by treating the discs as freely spinning rings. The maximum hoop stress in such a ring is given by

$$(Ts)max = \left(\frac{3+v}{4}\right)\rho w^2 \left(b^2 + \frac{1-v}{3+v} a^2\right),$$

where

b = outside radius = 0.3 inch

a = inside radius = 0.2 inch

ρ = density = 0.046 lb/in.^{3}

w = speed of rotation = 12,566 rad/sec

v = Poissan's ratio = 0.3 .

Evaluating the above equation for these parameters gives the tensile hoop stress as

$$(Js)max = 15\ 28 \text{ lb/in.}^2,$$

which is much less than the 10,000 lb/in.^{2} tensile strength of the polyimide material. The strain associated with this stress is

$$E = J/E = (1528/4.8 \times 10^5) \times 100 \text{ percent}$$
$$= 0.32 \text{ percent.}$$

The bismuth telluride layer would be subjected to essentially this level of strain. This is, however, an upper limit on strain level, since no support of the discs by the steel shell has been considered. In fact, the imposed strain should be much less than this value.

3. ACCELERATION STRESSES

The stresses due to the 120,000 g acceleration were estimated by considering the weight of the 0.3 inch high stack of discs, and distributing this force over the annular cross sectional area of these discs. The weight was determined as 0.00216 lb. At 120,000 g's this becomes 260 lb., and when distributed over the base of the discs gives a stress of 1655 psi. This is much less than the disc strength of about 10,000 psi.

4. THERMAL STRESSES

A upper bound on the thermal stress in the polyimide discs can be obtained from the equation

$$J = E \times \alpha T = (4.8 \times 10^{5})\ (2.85 \times 10^{-5})\ (400)$$
$$= 5472 \text{ psi},$$

which is less than the reported strength of the material. Perhaps of greater concern is possible cracking of the bismuth telluride layer due to differential thermal expansion relative to the polyimide substrate. The substrate expansion coefficient of 2.85×10^{-5} in./in./F is relatively high with respect to bismuth telluride, which is on the order of 1.0×10^{-5} in./in./F. Unless the expansion of the polyimide discs is restrained by the steel shell, the bismuth telluride layer will be placed in tensile stress.

Unfortunately, efforts to obtain mechanical properties of bismuth telluride were unsuccessful. Lacking such data, one would be unable to determine whether bismuth telluride can withstand a 400 F (222C) temperature cycle when subject to strains induced by a polyimide substrate.

5. COMMENTS ON STRUCTURAL INTEGRITY

Details of the design and assembly of the thermoelectric generator device have not yet been formulated. It is recommended that a more nearly complete stress study be made of the final configuration (to be developed in Phase II of this study). The preliminary structural analysis indicates that the polyimide substrate will not be overstressed for the anticipated service.

SECTION VII

DYNAMIC STABILITY ANALYSIS

The stability of a spin-stabilized projectile is a function of its spin angular momentum, the aerodynamic forces and moments, and the mass properties. The spin angular momentum is determined by the spin rate and the axial moment of inertia. The aerodynamic forces and moments are explicitly related to the exterior shape of the projectile, Mach number, dynamic pressure, Reynolds number, and location of the center of gravity. Thus it is seen that the mass properties influence both the angular momentum and the aerodynamics. In this brief analysis the effect of mass property variations on the stability of a 20mm proximity fuze projectile are to be considered. Unfortunately, these variations are related in a complex manner to the other factors influencing stability mentioned above.

In particular, this analysis is to consider the effects on stability of four mass properties, viz., axial moment of inertia (I_x), transverse moment of inertia (I_y), mass (m), and distance from the nose to the center of gravity (X_{cg}). There are two ways of viewing the stability and the influence of mass property changes. In the first, the effect on the damping coefficients λ_p and λ_n (see page 35 of Reference 2) is considered. Stability is attained when both coefficients are negative. For small mass property increments it is sufficient to investigate the coefficients with the smallest magnitude. For the cases to be considered below only the effect on λ_p is studied. The other stability criterion utilizes a plot of the generalized stability factor (s_d) and the gyroscopic stability factor (s_g). The plot is usually given as s_g^{-1} and s_d for the abscissa and ordinate, respectively. By definition the projectile is stable if the points on the plot are contained within an envelope defined by the equation

$$\frac{1}{s_g} = s_d(2-s_d).$$

These two means for viewing stability are equivalent. The advantage of the first is that it gives quantitative information on the distance required for a disturbance to dampen to some fraction of its initial amplitude. The second stability criterion can give insight into whether the projectile is near the boundary of the stability regime.

Instead of determining the stability for one or two sets of mass property parameters, a more general approach will be taken. The value of λ_p, s_g^{-1}, and s_d will be given at sea level conditions for two Mach numbers for the original proximity fuze missile designed by Motorola. In addition the partial derivatives of these three quantities will be shown with respect to I_x, I_g, M and X_{cg}/L (where L is body length). This will allow one to obtain the effect on stability of an arbitrary but small variation in the mass properties.

The reason for considering only sea level conditions is that stability problems will arise there first. Since dynamic pressure will decrease with altitude (if speed is constant), the projectile's stability will increase. This is because the sources of instability are certain ones of the aerodynamic moments (with static pitching moments being the major one), and these moments are proportional to the dynamic pressure.

Table V contains a list of the partial derivatives to be used in determining λ_p at Mach numbers 1 and 4. A new value of λ_p is determined by the formula

$$\lambda p = \lambda p_{nominal} + \sum_{i=1}^{4} \frac{\partial \lambda p}{\partial f_j} \Delta fj$$

where $\lambda p_{nominal}$ = value of damping coefficient for Motorola RF fuze design at appropriate Mach number, per caliber (see Table 5)

$f_1 = I_x$ slug-ft^2

$f_2 = I_y$ slug-ft^2

$f_3 = m$ slugs

$f_4 = X_{cg}/L$ -nondimensional

$\Delta f = f_{new} - f_{nominal}$.

TABLE V.
PARTIAL DERIVATIVES FOR DETERMINING λp (SEA LEVEL)

Mach No.	Nominal Values of λp	$\frac{\partial \lambda p}{\partial I_x} \times 10^4$	$\frac{\partial \lambda p}{\partial I_y} \times 10^4$	$\frac{\partial \lambda p}{\partial m} \times 10^4$	$\frac{\partial \lambda p}{\partial (X_{cg}/L)} \times 10^4$
1	-0.757×10^{-4}	0.135×10^6	0.00432×10^6	-113.6	-0.385
4	-0.471×10^{-4}	-0.795×10^6	0.0134×10^6	251	-5.6

TABLE VI.
PARTIAL DERIVATIVES FOR DETERMINING S_g^{-1} (SEA LEVEL)

Mach No.	Nominal Value	$\frac{\partial S_g^{-1}}{\partial I_x}$	$\frac{\partial S_g^{-1}}{\partial I_g}$	$\frac{\partial S_g^{-1}}{\partial m}$	$\frac{\partial S_g^{-1}}{\partial (X_{cg}/L)}$
1	0.0792	-0.0543×10^6	0.00698×10^6	0	-0.3438
4	0.635	-0.221×10^6	0.0121×10^6	0	-1.19

TABLE VII.
PARTIAL DERIVATIVES FOR DETERMINING S_d (SEA LEVEL)

Mach No.	Nominal Value	$\frac{\partial S_d}{\partial I_x}$	$\frac{\partial S_d}{\partial I_y}$	$\frac{\partial S_d}{\partial m}$	$\frac{\partial S_d}{\partial (X_{cg}/L)}$
1	0.702	-0.0261×10^6	0.00902×10^6	0	-1.896
4	0.634	-0.104×10^6	0.0070×10^6	-61.1	-1.45

TABLE VIII.
EFFECT OF MASS PROPERTY CHANGES ON THE STABILITY PARAMETERS

	Original Values			New Values		
Mach No.	λ_p	S_g^{-1}	S_d	λ_p	S_g^{-1}	S_d
1	-0.757×10^{-4}	0.0792	0.702	-0.757×10^{-4}	0.0802	0.715
4	-0.471×10^{-4}	0.635	0.634	-0.466×10^{-4}	0.603	0.629

The nominal values and partial derivatives required to calculate new values of S_g^{-1} and S_d are found in Tables VI and VII. The formula given above is used with either S_g^{-1} or S_d in place of λ_p.

Figure 21 shows a plot of S_g^{-1} versus S_d and the points for the Motorola RF fuze design at Mach numbers 1 and 4.

For the new projectile with the thermoelectric powered fuze, the following mass property increments were calculated

$$\Delta I_x = 0.08\times10^{-6} \text{ slug-Ft}^2$$
$$\Delta I_y = 0.51\times10^{-6} \text{ slug-Ft}^2$$
$$\Delta m = 0.129\times10^{-3} \text{ slug}$$
$$\Delta X_{cs}/L = -0.00532$$

where a positive increment denotes that the new projectile's value of that parameter is higher than the one with the battery. The old and new values of λ_p, S_g^{-1}, and S_d at Mach numbers 1 and 4 are given in Table VIII. It is seen that the effect of the design modifications is practically negligible. In fact no attempt was made to plot the new values in Figure 20 since the points would be almost on top of the original ones.

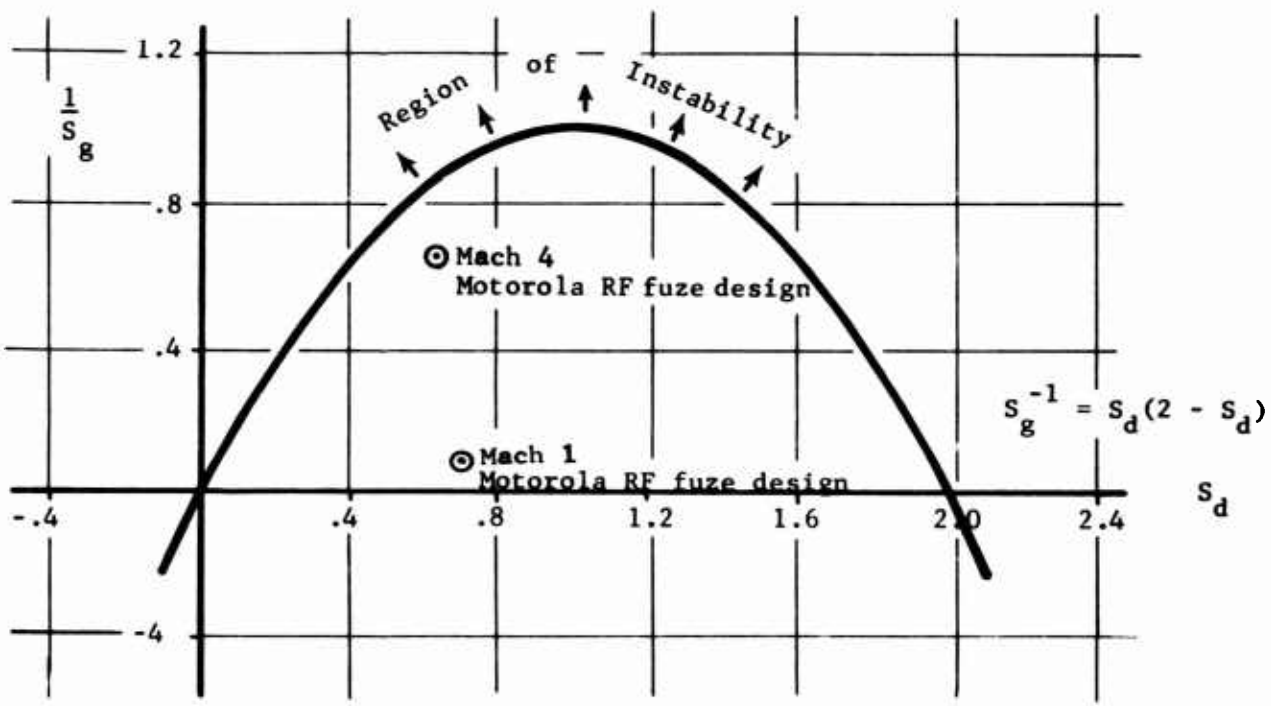

FIGURE 20. STABILITY PLOT, S_g^{-1} vs S_d

SECTION VIII

COST EFFECTIVENESS OF THERMOELECTRIC CONVERTER

The purpose of this task was to explore alternative thermopile manufacturing approaches. In view of the size of the thermoelectric elements required for this application, thin film fabrication techniques will be required. Several techniques for vapor deposition of bismuth telluride including flash vapor deposition and DC sputtering, were considered. The DC sputtering technique was selected for use in preliminary studies based on the higher degree of control afforded and the potential for mass production manufacturing techniques. The principal disadvantage of sputtering is that it requires 6 to 12 hours to deposit 0.002-in.-thick thermoelectric elements. However, commercial sputtering equipment would permit depositing bismuth telluride on up to 10,000 disc modules simultaneously.

The steps involved in the evaluation of the cost effectiveness of thin film manufacturing methods included investigating alternative

- Substrate (disc) materials
- "Masking" techniques
- Hot-strap and cold-strap deposition methods
- Sputtering parameters.

Vespel was identified as a suitable substrate material for use in the fabrication of disc modules during Phase II of this study. Vespel was selected because of (1) its ability to withstand exposures to temperatures of up to 500 F,(260C), (2) its availability in the required thickness (0.035 in.), and (3) its low thermal conductivity.

Studies also revealed that the dimensions of the conductive straps (which connect the p- and n-type thermoelectric elements and wrap around the edge of the substrate) are large enough that it may be possible to deposit the straps by the standard silk-screen-and-fuze process. Otherwise, thermal evaporation of conductive metal through a mask may have to be employed to deposit the straps.

The investigation of both sputtering parameters and the effectiveness of alternative masking techniques was undertaken and involved preliminary

sputtering trials. First, bismuth telluride bar stock (supplied by Melcor) was diced into 1 in. x 2 in. x 0.062 in. sections in order to make up a 4 in. diameter "target" for use in BCL's sputtering equipment. This bismuth telluride target provided for the deposition of 0.001 in. to 0.002 in. thick layers of bismuth telluride on selected substrates. These preliminary deposition studies provided an important input to the study of cost effective thermopile manufacturing approaches as well as direction for the prototype converter development scheduled for Phase II of this study.

Next, Bi_2Te_3 (p-type) was sputtered onto glass slides by using stainless steel masks. Two identical masks were made with the EDM (Electrical Discharge Machine) method. The overall size of the masks was 1 x 2 x 0.008 in. The slots cut in the mask was 0.100 in. long x 0.025 in. wide. Three of these slots had a space of 0.065 in. between them and the fourth had a space of 0.020 in. Another form of mask which consisted of metal strips 0.25 in. wide x 1.0 in. long and 0.003 in. thick was used. These were clamped over glass slides with a space between the strips of 0.125 in.

The parameters for sputtering the Bi_2Te_3 were as follows:

Cathode-Substrate distance — 2.5 in.
Cathode material — 1 in. x 1 in. Bi_2Te_3 (p-type) positioned on top of a 4-in.-diameter iron plate
Base pressure — 5×10^{-6} torr
Air pressure — 40 μ
Foreline pressure — 200 μ
Cathode voltage — 2.5 Kv
Cathode current — 40 ma
Power — 100 watts
Cathode power density — 8 watts/in.^{2}
Deposition rate — 280 Å/min
Deposition time — 15 hr.

Measurements of the coating thickness were made with a Talysurf. As was expected, the coating through the mask was rounded near the edges.

Sputtered bismuth telluride elements of dimensions and separation distance representative of the actual disc converter are illustrated in Figure 21. As indicated above, a stainless steel "physical" mask was used in the sputtering of these thin film thermoelements. The significance of these results is that less costly physical masking techniques can be used in the thin-film deposition of bismuth telluride.

Electrical property measurements were made in order to characterize the sputtered thin film thermoelements. These measurements were made on 0.125 in. wide x 0.80 in. long films which ranged in thickness from 0.0005 in. to 0.001 in. The results of preliminary measurements indicate that the Seebeck coefficient of sputtered films is within 15 percent of that of the bismuth telluride source material. The electrical resistivity measurements, however, indicate that the films have a factor of two or more higher electrical resistivity than the bulk material. Microscopic inspection of the thin films indicated that most of the samples exhibited microcracks. This microcracking likely contributed to the high electrical resistivity. Analysis of the sputtering system revealed that the glass slides probably heated up to 200 C (380 F) or more during the sputtering process. This high temperature combined with the different thermal expansion rates of the bismuth telluride and the glass slide likely led to excessive stresses, and, hence, cracking in the thermoelectric material. The only elements that were not cracked were the smaller 0.25 in. wide x 0.100 in. long elements. However, these smaller elements were deposited in a second sputtering series which did not provide representative p-type bismuth telluride films. This was due to the fact that the "target" was fabricated by using bismuth telluride wafer segments which were not in good thermal contact with the target base and, hence, the water cooled heat sink. By overheating, the more volatile species of bismuth telluride evaporated during the earlier sputtering trial--thereby disproportioning the bismuth telluride alloy. This problem can be readily overcome by fabricating a monolithic bismuth telluride target and achieving good thermal contact with the water cooled heat sink.

Reproduced from best available copy.

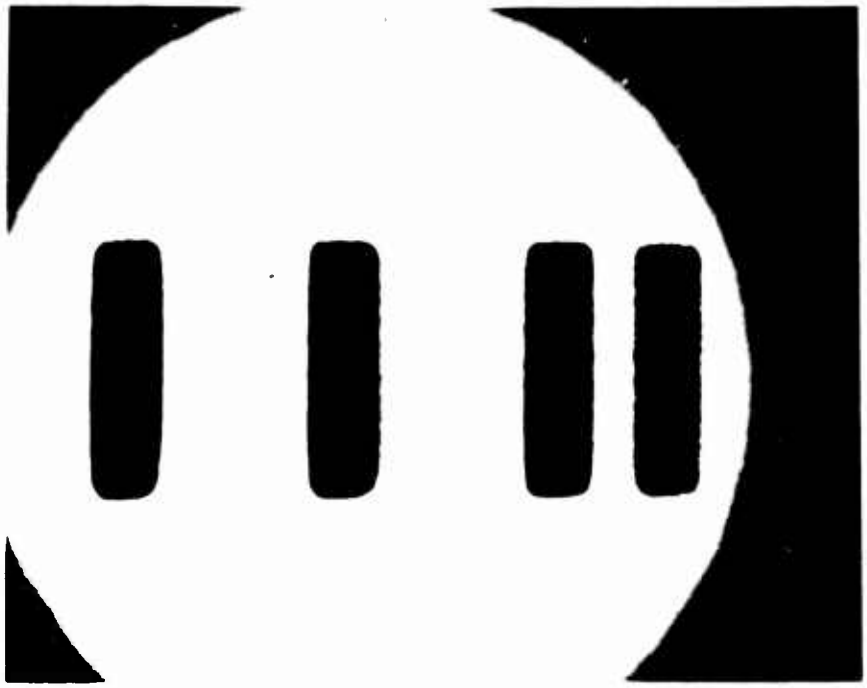

13X

FIGURE 21. PHOTOGRAPH OF SPUTTERED BISMUTH TELLURIDE FILMS (0.100 IN LONG X 0.025 IN WIDE X 0.0005 IN THICK)

A preliminary estimate has been made of the costs of fabricating the selected disc thermoelectric modules involving bismuth telluride. These very preliminary estimates are summarized in Table 9 and indicate that the total thermoelectric convertor may be fabricated for less than $1.80 per convertor (containing 7 modules). These estimates have been made conservative by assuming a twc year payback on capital equipment, 200 working days per year, two runs per day per set of equipment where , where a run equals 10,000 disc convertors. Further refinement of the cost analysis is not warranted due to the uncertainty in ultimate deposition processes and substrate material. However, it does indicate an approximate figure for the convertor concept in its present stage of development.

TABLE IX.
APPROXIMATE COST BREAKDOWN
FOR DISC THERMOELECTRIC CONVERTORS

Item	Materials Cost, $	Labor Cost, $	Unit Disc Cost, $
Bismuth Telluride	200/lb.	--	0.0266
Vespel Substrate	10/in.^{3}	--	0.0600
Sputtering Equipment*	--	--	0.0375
Electrode Deposition Equipment+	--	--	0.012
Supporting Labor**	--	$15/hr.	0.108
Building Rental, Other Costs x			
Total Cost Per Convertor			$ 1.79

* Assume $3000,000 for equipment plus automatic mask/disc handling equipment

\+ Assume $100,000 for thick film equipment.

** Three workers per shift, three shifts.

x Based on $100,000 per annum costs.

SECTION IX

SAFETY ANALYSIS

The aerodynamically heated thermoelectric convertor concept developed in this study has also been analyzed from the standpoint of safety during ground handling, storage, transportation, and firing. One existing feature of the projectile is the "spin-back" safety measure, which prevents arming the projectile until the rotational effects of firing "arm" the firing pin. In addition to this feature, the aerodynamically heated thermoelectric power supply offers an additional measure of safety to its users. This second safety feature derives from the fact that the RF proximity fuze is not activated until a threshold voltage (and current) is developed within thermoelectric convertor. In order to develop the necessary voltage/current output from the convertor, a sufficiently large heat flux (>10.0 Btu/sec. ft^2 or 13.0 watts/cm^2) must be applied and sustained for at least 50 to 100 msec.

In the event the thermoelectric-powered RF proximity fuzes were exposed to a fire (e.g., often simulated by a 1450 F (790 C) radiant source), the heat flux would reach only about 6 watts/cm^2. This heat flux is only about one half the heat flux required to develop the threshold voltage necessary to activate the RF proximity fuze. Hence, in the event of a fire, the projectile tip will heat up without developing a significant temperature gradient within the thermoelectric converter. At some point, a fire will heat the RF proximity fuze components to temperatures beyond the operational limits of the electronic components. For example, the Vespel substrates will thermally decompose above 500 F (260 C). The electronic components in the RF circuit will fail rapidly as the temperatures approach these temperatures.

Another measure of safety provided by the thermoelectric-powered fuze is the safe arming distance. This distance is dictated by the thermal inertia of the thermoelectric convertor in the presence of the imposed aerodynamic heating rate. Based on analyses discussed in Part 7 of Section VI (See Table 4), the safe arming interval is at least 50 msec or about 150 feet.

The incidence of "hung rounds" will not activate the thermoelectric-powered RF proximity fuze unless the temperature of the projectile environment reaches or exceeds 1800 F (990 C). Heating or cooling of the projectile prior to firing will not significantly affect the time history of the temperature difference developed across the convertor via aerodynamic heating. However, the ultimate hot junction of the convertor will depend on the initial projectile temperature. It should be noted that the output voltage developed has a first order dependence on the temperature difference across the convertor. Therefore, since the safe arming distance depends on the time history of the convertor output voltage, it follows that the safe arming distance will be relatively insensitive to the initial temperature of the projectile.

SECTION X

CONCLUSIONS AND RECOMMENDATIONS

During the seven month period of this Phase I study, a number of analyses have been performed aimed at assessing the feasibility of utilizing aerodynamically heated thermoelectric convertors to power previously developed[2] RF proximity fuzes. The collective results of this study indicate that such a thermoelectric power supply is feasible and can be made compatible with the existing RF proximity fuze--in terms of both the fuze voltage/current requirements and the safe arming distance desired.

The principal findings from this study include:

- 20 mm RF proximity fuze may be powered with as little as 40 mw at an input voltage of 7.5 volts.
- Bismuth telluride is the most attractive thermoelectric material for the number of couples required and the threshold aerodynamic heat flux required.
- Disc thermoelectric module concept may offer a cost effective means for distributing 200 to 400 couples over the available surface area on the 20-mm projectile.
- Aircraft should have an airspeed of at least 80 mph and not more than 760 mph in order to provide 2.5 seconds of active power to the RF fuze circuit while flying at 3000 feet and firing at -20 degrees.
- At significantly higher altitudes (>25,000 feet), the above airspeed limits will be somewhat lower but trajectory lifetimer of up to 3.5 seconds may be possible--without any energy storage.
- At increasingly lower altitudes and airspeeds above 80 mph, there is an increasing incentive to use energy storage to provide excess energy produced during early phase of trajectory for later phase of trajectory.

- Electrical (capacitor) storage is one means for extending the active life of the RF proximity fuze. However, physical size limitations within 20-mm projectile tip provide increases in trajectory of only 0.5 seconds.
- Preliminary structural analysis indicates that the polyimide substrate will not be overstressed for the anticipated service. However, the effects of differential thermal expansion between the Vespel and the bismuth telluride thermoelectric elements pose some uncertainties at this time.
- Dynamic stability analyses of the modified projectile tip indicate that the changes in center of mass, moment of inertia, and mass of projectile tip are sufficiently small to have a negligible effect on the dynamic stability of the overall projectile.
- Preliminary safety analysis indicates that the thermoelectric convertor requires a sufficiently high heat flux (to produce threshold power for fuze) to minimize the chance that accidental fires or "hung" rounds will activate fuze.
- Preliminary thin film deposition studies indicate that bismuth telluride can be sputtered in the required dimensions by using relatively low cost physical masking techniques. Electrical property measurements on these preliminary trial depositions revealed the Seebeck coefficient to be within 15 to 20 percent of that of the bulk material. The electrical resistivity, however, was a factor of two or more larger than that of the bulk material. The high resistivity of these samples has been traced, in part, to microcracks in the thin film specimens--possibly due to differential thermal expansion of bismuth telluride with respect to the glass substrate.
- 30 mm RF proximity fuze can be powered by aeroheated thermoelectric convertors for trajectory durations of at least 3.5 seconds owing to its larger projectile mass.

Based on the above findings, it is concluded that aerodynamically heated thermoelectric convertors provide a feasible source of power for RF proximity fuzes in 20 mm and 30 mm projectiles. Certain technical uncertainties exist, however, at this phase of the concept development:

- Which deposition method is best suited to this task upon considering the need for high volume/low cost production and high figure-of-merit material?
- Can bismuth telluride in 0.1 in. lengths withstand the differential thermal expansion effects associated with the use of Vespel substrates?
- Can acceptably low resistivity material be deposited without the need for annealing (sintering) following deposition?
- What effects will long term storage of 20 mm projectiles have on the thermoelectric convertors? Will moisture and heat and cold have any effects?

On the basis of the findings of this Phase I study, it is recommended that a Phase II study be initiated emphasizing

- Refinement of thin film deposition of bismuth telluride on polyimide substrates including enhanced cooling of target and substrate during sputtering.
- Characterization of deposited bismuth telluride thermoelements, before and after thermal cycles simulating several seconds at a heat flux of 13 to 15 watts/cm^2.
- Optimization of deposition parameters, substrate preparation, and electrode configuration.
- Evaluation of prototype projectile tips incorporating disc thermoelectric modules including output voltage, current, and hot and cold junction temperatures as functions of time during 1.5 to 2.5 second simulated trajectories.

REFERENCES

1. "Power Converter Nose Cone", Final Report, prepared by Grumman Aerospace Corporation for the U.S. Air Force under Contract No. F08635-72-C-0012 (January, 1973).

2. "Air-to-Surface Proximity Fuze for 20 mm Projectile (U)", Contract AFATL-TR-73-20, Work performed by Motorola, Inc. (1973).

3. Personal communication received from Lt. James M. Howard, Energy Conversion Research Laboratory (LE), Aerospace Research Laboratories (AFSC), Wright-Patterson Air Force Base, Ohio 45433.

4. Chang, S., Energy Conversion, Prentice Hall Publishing Company (1962).

5. Lyons, C. W., "Hypersonic Laminar and Turbulent Heat Transfer for Slightly Blunted Slender Cones", Ph.D. Thesis, University of Maryland (1969).

6. Wilson, R.E., "Laminar Boundary Layer Growth on Slightly Blunted Cones at Hypersonic Speeds", J. Spacecraft and Rockets, Vol. 2, pp 490-496 (1965).

7. Hastings, S. M. and Chones, A. J., "Supersonic Aerodynamic Heating of a Tamed Sphere-Cone Windtunnel Model", U.S. Naval Ordnance Laboratory, NAVORD Dept. 6812 (November, 1960).

8. Ragsdale, N.C., Brown, M.A., Ball, R. G., "An Experimental Investigation of the Laminar Boundary Layer on a Spinning Ogive Cylinder in Supersonic Flow", Naval Ordnance Lab., NOLTR 72-265 (November, 1972).

9. Teteruin, N., "An Empirical Equation for Prediction of Transition Location on Cones in Supersonic or Hypersonic Flight", U.S. Naval Ordnance Laboratory, NOL TR73-127 (June, 1973).

10. Trimpi, R. L., Gallagher, J.G., and Jones, R.A., "Heat Transfer Tests of 20 mm Projectiles at a Mach Number of 5 With an Analysis by Unsteady Scaling Laws to Predict Component Temperature Rises After Firing for Various Free-Flight Conditions", NASA TN D-758 (1961).

11. Garrett, W.A., "Muzzle Velocity Uniformity Investigation:, AMCMS Code: 552C.11.22507.03, Product Assurance Directorate, Frankford Arsenal (November, 1973).

APPENDIX A

DESCRIPTION OF THE COMPUTER PROGRAM TRUMP

APPENDIX

DESCRIPTION OF THE COMPUTER PROGRAM TRUMP

TRUMP solves a general nonlinear parabolic partial differential equation describing flow in various kinds of potential fields, such as fields of temperature, pressure, and electricity and magnetism; simultaneously, it will solve two additional equations representing, in thermal problems, heat production by decomposition of two reactants having rate constants with a general Arrhenius temperature dependence. Steady state and transient flows in one, two, or three dimensions are considered in geometrical configurations having simple or complex shapes and structures. Problem parameters may vary with spatial positions, time, or primary dependent variables--temperature, pressure, or field strength. Initial conditions may vary with spatial position, and among the criteria that may be specified for ending a problem are upper and lower limits on the size of the primary dependent variable, upper limits on the problem time or on the number of time steps or on the computer time, and attainment of steady state. Solutions may be obtained by use of explicit or implicit difference equations, or by an optimized combination of them.

☆U.S.Government Printing Office: 1975 — 657-020/531